March 1993   1/9/84 to 1/9/86

Analytical and Experimental Investigation of Annular   Contract F33615-81-C-3078
Propulsive Nozzles   P.E. 62203F
                                                             P.R. 3012
                                                             TA 13
R.R. Conley - McDonnell Douglas Astronautics   WU 89
J.D. Hoffman, H.D. Thompson, Purdue University

McDonnell Douglas Astro. Co.   Purdue University
St. Louis Division   West Lafayette IN 47907
St. Louis MO 63166

Aero Propulsion and Power Directorate
Wright Laboratory
Air Force Materiel Command   WL-TR-93-2048
Wright-Patterson AFB OH 45433-7655
WL/POPR, ATTN: Smith (513) 255-2175

Journal Article

The final report consists of AIAA papers. The report presents an analytical
performance prediction methodology for annular propulsion nozzles with and without
swirl introduced in the combustor upstream of the nozzle. Four types of
swirlers were investigated: free vortex, constant angle, forced vortex and
Rankine vortex swirlers. For the no-swirl case thrust efficiencies and static
pressure profiles from cold flow testing of selected nozzles are summarized
and compared to the predictions.

93   4 06 067

Ramjets, Supersonics   34

Unclassified   Unclassified   Unclassified   UL

NOTICE

WHEN GOVERNMENT DRAWINGS. SPECIFICATIONS. OR OTHER DATA ARE USED FOR ANY PURPOSE OTHER THAN IN CONNECTION WITH A DEFINITELY GOVERNMENT-RELATED PROCUREMENT. THE UNITED STATES GOVERNMENT INCURS NO RESPONSIBILITY OR ANY OBLIGATION WHATSOEVER. THE FACT THAT THE GOVERNMENT MAY HAVE FORMULATED OR IN ANY WAY SUPPLIED THE SAID DRAWINGS. SPECIFICATIONS. OR OTHER DATA. IS NOT TO BE REGARDED BY IMPLICATION. OR OTHERWISE IN ANY MANNER CONSTRUED. AS LICENSING THE HOLDER. OR ANY OTHER PERSON OR CORPORATION; OR AS CONVEYING ANY RIGHTS OR PERMISSION TO MANUFACTURE. USE. OR SELL ANY PATENTED INVENTION THAT MAY IN ANY WAY BE RELATED THERETO.
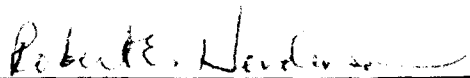
THIS TECHNICAL REPORT HAS BEEN REVIEWED AND IS APPROVED FOR PUBLICATION.

JOHN R. SMITH, Project Engineer
Propulsion Development Branch
Advanced Propulsion Division

WILLIAM C. BURSON, JR., Chief
Propulsion Development Branch
Advanced Propulsion Division

ROBERT E. HENDERSON, Chief
Advanced Propulsion Division
Aero Propulsion & Power Directorate

IF YOUR ADDRESS HAS CHANGED. IF YOU WISH TO BE REMOVED FROM OUR MAILING LIST. OR IF THE ADDRESSEE IS NO LONGER EMPLOYED BY YOUR ORGANIZATION PLEASE NOTIFY WL/POPR , WRIGHT-PATTERSON AFB. OH 45433-7655 TO HELP MAINTAIN A CURRENT MAILING LIST.

COPIES OF THIS REPORT SHOULD NOT BE RETURNED UNLESS RETURN IS REQUIRED BY SECURITY CONSIDERATIONS. CONTRACTUAL OBLIGATIONS. OR NOTICE ON A SPECIFIC DOCUMENT.

AIAA'84

AIAA-84-0282

An Analytical and Experimental Investigation of Annular Propulsive Nozzles

R.R. Conley, McDonnell Douglas Astronautics Co., St. Louis, MO; and J.D. Hoffman and H.D. Thompson, Purdue Univ., West Lafayette, IN

X
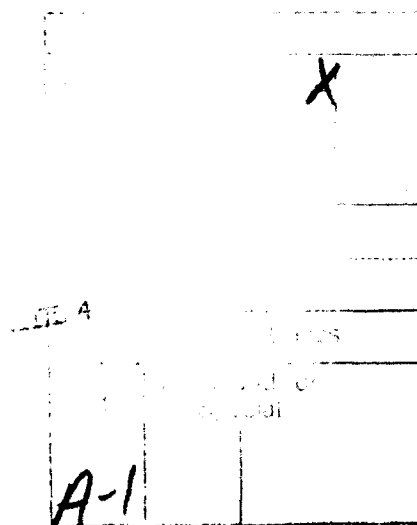
A-1

AIAA 22nd Aerospace Sciences Meeting

January 9-12, 1984/Reno, Nevada

AN ANALYTICAL AND EXPERIMENTAL INVESTIGATION
OF ANNULAR PROPULSIVE NOZZLES*

Ralph R. Conley[t]
McDonnell Douglas Astronautics Company - St. Louis Division
St. Louis, Missouri 63166

and

Joe D. Hoffman[tt] and H. Doyle Thompson[ttt]
Purdue University
West Lafayette, Indiana 47907

Abstract

This paper discusses an analytical performance prediction methodology for annular propulsive nozzles and the application of that methodology to selected nozzles. Thrust efficiencies and static pressure profiles from cold flow testing of the selected nozzles are summarized and compared to the predictions. These comparisons show that the analytical methods are reasonably accurate if the radial velocity components in the transonic region of annular nozzles are small. The areas of prediction/test disagreement are identified for future improvements.

Nomenclature

A	Area
ASME	American Society of Mechanical Engineers
C_D	Discharge Coefficient
IVL	Initial Value Line
m	Mass Flow Rate
MOC	Method of Characteristics
NPR	Nozzle Pressure Ratio
NTS	Nozzle Test Stand
P	Pressure
VNAP	Viscous Nozzle Analysis Program
Y	Ratio of Specific Heats
n	Efficiency

Subscripts

a	Ambient
act	Actual
AR	Area Ratio
B	Base
C	Cowl
e	Exit
I	Internal
o	Stagnation
p	Centerbody (plug)
PR	Pressure Ratio
ref	Reference
t	Throat
*	Choking

Introduction

The conventional propulsive nozzle is an axisymmetric converging-diverging design and has been used successfully in rocket, turbojet and ramjet engines for many years. The advantages of such nozzles include efficient design-point performance, reasonable weight and cost and the availability of accurate design/analysis techniques. On the other hand, the disadvantages of such nozzles include excessive length and inefficient off-design performance.

Several annular nozzle concepts, formed by inserting axisymmetric centerbodies within conventional nozzles, have been considered to overcome these disadvantages. As depicted in Figure 1, the centerbody may be located either upstream, downstream or in the throat plane of the conventional nozzle. The objective of the present work was to conduct analytical and experimental investigations of selected annular nozzles to acquire a better understanding of the flow processes and performance potential of these concepts.

This paper presents the results of this work for five annular nozzles which encompass the design options noted in Figure 1. Primary emphasis is on an analytical performance prediction methodology for such nozzles and the application of that methodology. The results of considerable cold flow testing of selected nozzle models are summarized and compared with the analytical predictions.

All analytical performance predictions presented in this paper were made prior to nozzle model cold flow testing. No revised predictions based on post-test, "fine tuned" reruns of the analytical codes are included. Therefore, the comparisons with experimental data show both the strengths and weaknesses of the basic prediction methodology. Some additional capabilities which would enhance the prediction methodology are identified as areas for future improvements.

Cold Flow Testing

Annular nozzle model cold flow testing was conducted in the McDonnell Aircraft Company Nozzle Test Stand (NTS). The nozzle driven ejector assembly was used during testing to obtain performance data at higher pressure ratios. A brief description of the NTS and ejector assembly are presented in this section.

CENTERBODY UPSTREAM

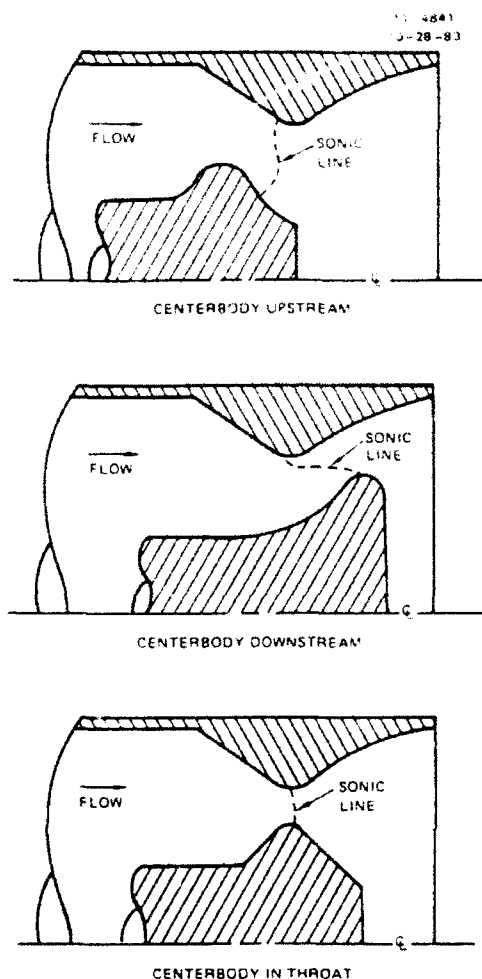CENTERBODY DOWNSTREAM

CENTERBODY IN THROAT

Fig. 1   Annular nozzle concepts.

The NTS, depicted in Figure 2, was developed to provide precise measurements of nozzle thrust and flow rate. Test nozzles are attached to a plenum assembly which is mounted between the arms of a double armed pendulum. Pressure regulated, dry air is supplied to the plenum by dual supply lines which run parallel to the pendulum arms. Thus, the incoming air is perpendicular to the nozzle thrust axis and its momentum does not influence the thrust measurement.

An ejector assembly, also depicted in Figure 2, is used with the NTS to increase nozzle pressure ratio (plenum pressure/back pressure) capability. The exhaust flow from the test nozzle drives the ejector and lowers the nozzle back pressure below the ambient pressure.

Nozzle model thrust during testing is measured by recording the deflection of the pendulum about the I-beam flexure with a linear variable differential transformer (LVDT). The thrust magnitude is determined by multiplying the deflection distance by the deflection constant which is determined prior to each test series using dead weight loading with a pulley arrangement. The air supply lines are pressurized during the calibration process. Thus, tare forces due to thrust and pressure loads are included in the calibration data.
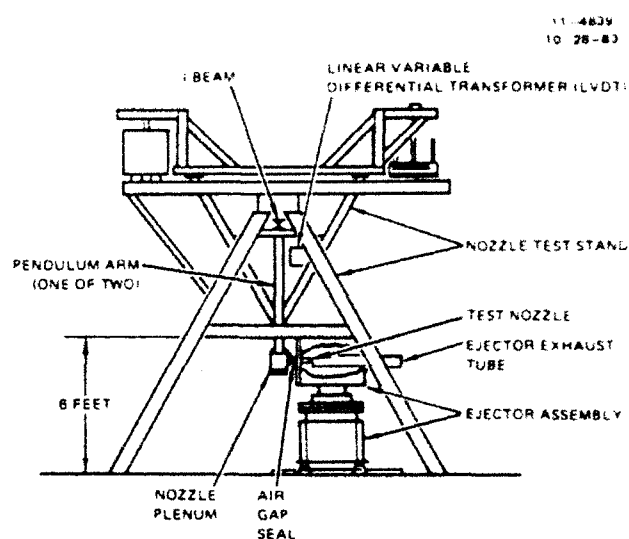
Fig. 2   Nozzle test stand.

The thrust measurement accuracy of the NTS for nozzles exhausting into the atmosphere (i.e., without the ejector) were verified by tests with an American Society of Mechanical Engineers (ASME) standard nozzle. These nozzles are commonly used to verify thrust measurement facilities since the thrust efficiency is easily calculated with one-dimensional theory. As shown in Figure 3, a curve fit of data from a typical verification test series with the ASME nozzle is approximately 0.4 percent below the theoretical line. This excellent correlation confirms the accuracy of the NTS thrust measurement method.
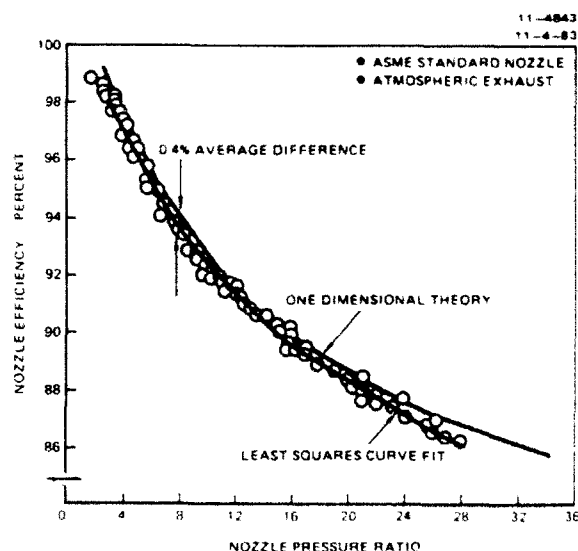

Fig. 3   NTS thrust measurement evaluation summary.

Thrust measurement capability of the NTS with the ejector was verified by comparing nozzle efficiency data between runs exhausting into the atmosphere and runs exhausting into the ejector. Such comparisons for a conical nozzle are presented in

Figure 4 and show excellent agreement between the ejector and atmospheric exhaust runs, verifying the thrust measurement capability of the NTS with the ejector.
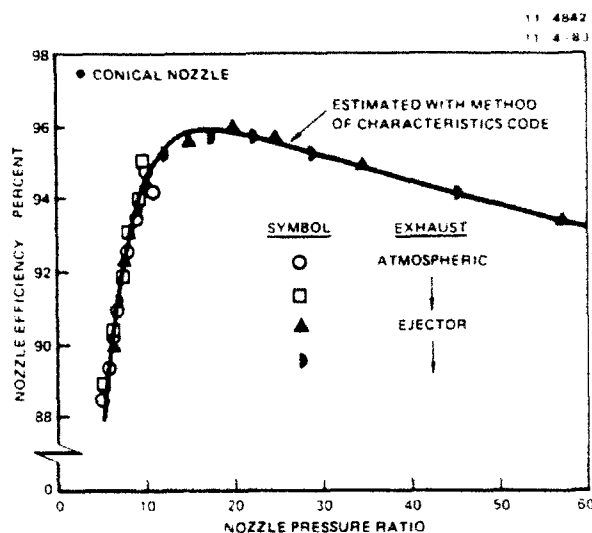

11-4842
11-4-83

Fig. 4 NTS thrust measurement evaluation summary.

The mass flow rate through the test nozzle is metered through a choked venturi which was calibrated by the Colorado Engineering Experimental Station. Air temperature and pressure measurements in the venturi are made to correct for real gas effects on mass flow rate.

Four annular nozzles which encompass the design options noted in Figure 1 were selected for model fabrication and cold flow testing. The internal contours of these nozzles were developed by various design techniques[1,2]. An additional nozzle model was also fabricated based on the design improvement study described later in this paper.

Figure 5 summarizes the nozzle model cold flow performance testing conducted in the NTS facility. The nozzle model and the number of test runs conducted with atmospheric and ejector exhaust conditions are summarized. Twenty test runs were made and data were recorded at 8 to 10 values of nozzle pressure ratio for each run.

11-4840
10-28-83

NOZZLE MODEL	NUMBER OF RUNS		
	EXHAUST		TOTAL
	ATMOSPHERE	EJECTOR	
N1	-	2	2
N2	3	3	6
N3	2	3	5
N4	1	2	3
N5	-	4	4
TOTAL NUMBER OF RUNS			20

Fig. 5 Cold flow test summary.

Performance Prediction Methodology

The propulsive nozzle is the thrust producing component of jet propulsion engines such as rockets, turbojets and ramjets. The function of the propulsive nozzle is to convert the random thermal energy of the gases entering the nozzle into directed kinetic energy at the nozzle exit, thus creating a thrust on the propulsive system. The expansion process must be accomplished as efficiently as possible, since the gross thrust developed by the nozzle is directly related to the nozzle exhaust velocity. For rocket engines, the gross thrust produced by the nozzle is also the net thrust. However, for airbreathing engines (turbines and ramjets), the net thrust is the difference between the nozzle gross thrust and the inlet ram drag. Consequently, all losses in nozzle gross thrust for airbreathers are magnified several times in net thrust and it is imperative that the nozzle efficiency be as large as possible.

Figure 6 illustrates the thrust producing components of a generic annular nozzle. The nozzle thrust is composed of the thrust developed across the throat T_T, the thrust developed by the pressure acting on the cowl surface T_C, the thrust developed by the pressure acting on the centerbody surface T_P and the thrusts acting on the centerbody base area T_{PB} and the annular base area around the nozzle exit T_{CB}.
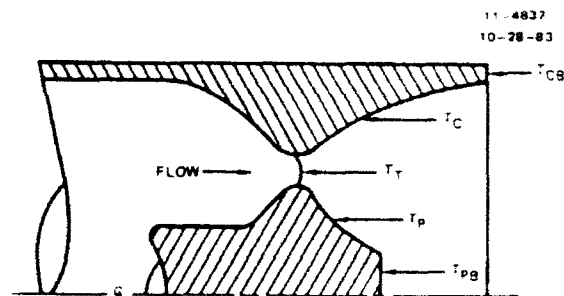

11-4837
10-28-83

Fig. 6 Thrust components of an annular nozzle.

The relative magnitudes of these thrust components depend on the nozzle design. For nozzle geometric area ratios between 3:1 to 5:1, as considered in this study, the magnitude of the throat thrust is approximately 80 percent of the nozzle ideal thrust, the cowl thrust is from 10 to 15 percent of the ideal thrust and the centerbody and base thrusts and losses comprise the remainder. However, if the throat flowfield has a large radially inward or outward component, the axial component of the throat thrust is reduced considerably and the cowl and centerbody thrust components become a larger portion of the total thrust.

The accuracy and efficiency of nozzle performance prediction techniques are highly dependent on the flowfield model chosen to represent the actual flowfield. In the present study, the flowfield model is based on the following assumptions:
(1) steady axisymmetric flow,
(2) inviscid nonconducting fluid with no body forces,
(3) thermally and calorically perfect gas and
(4) separation and base pressures selected from empirical correlations.

3

The governing equations consist of the continuity equation, the component momentum equations, the energy equation and the thermal and caloric equations of state. A detailed discussion of these equations is presented in Reference 3.

The choice of a numerical method, or methods, to solve these governing equations is also crucial to the success of the performance prediction procedure. A subsonic/transonic solution is required to define the throat thrust, while a supersonic solution is required to define the cowl, centerbody and base thrusts. Experience has shown that subsonic/transonic flowfields can be adequately determined by finite difference approaches, whereas the method of characteristics is the most accurate approach to determining supersonic flowfields in nozzles. Therefore, the numerical methods selected for the performance prediction procedure in the present study are a finite difference approach, as employed in the VNAP code[4], to define the subsonic/transonic flowfield and a method of characteristics approach, denoted as the MOC code[5], to define the supersonic flowfield.

Performance Prediction Example

The application of the selected performance prediction methodology to nozzle N1, see Figure 7, is presented in this section. The flowfield solutions obtained from the VNAP and MOC codes are presented and the calculations of throat, cowl, centerbody and base thrusts are described in detail. Comparisons with cold flow test data are also made.
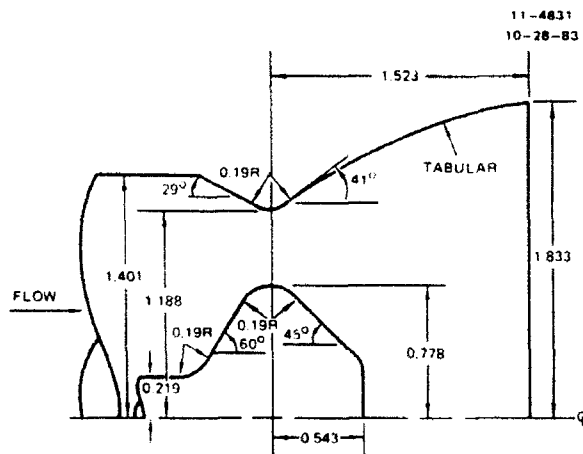
Fig. 7 Geometry of nozzle N1.

Figure 7 depicts the geometry of nozzle N1. The nozzle has an axisymmetric cowl consisting of a cylindrical upstream section, a conical-circular arc shoulder section and a contoured downstream section. The axisymmetric centerbody has a cylindrical upstream support section, a conical initial section, a circular arc shoulder, a conical section downstream of the shoulder and a flat aft facing base. Note that the shoulder sections of the cowl and centerbody are at the same axial station.

As previously mentioned, the subsonic/transonic solution obtained from the VNAP code defines

the nozzle throat flowfield. Figure 8 illustrates the Mach number distribution in the throat region of nozzle N1 as an example of the flowfield definition provided by the VNAP code. From this definition, the throat thrust is determined by integrating the momentum flux and pressure forces across a selected line that spans the throat in the slightly supersonic region. This same line, denoted as the initial value line (IVL), is then used to start the MOC code solution of the supersonic flowfield.
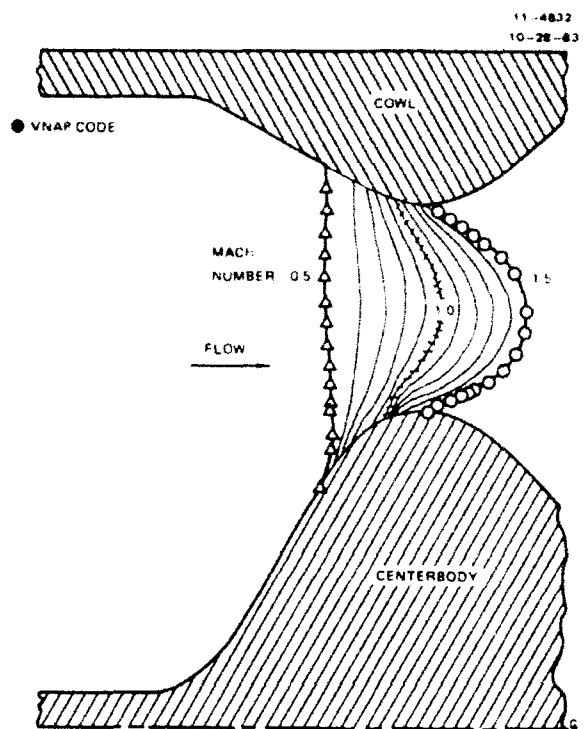
Fig. 8 Mach number distribution for nozzle N1.

The thrusts developed by the pressures acting on the cowl and centerbody surfaces are determined by integrating the axial components of the pressure forces acting on these surfaces. The pressure distributions along the cowl and centerbody surfaces are obtained from the supersonic flowfield solution provided by the MOC code. The MOC code constructs the flowfield solution along the previously mentioned IVL, beginning at the cowl and proceeding along the IVL to the centerbody surface. The code continues the solution along the centerbody surface until a specified separation pressure is reached. At this point, a free-pressure boundary is calculated and projected to the nozzle axis. Left-running Mach lines emanating from these boundaries are propagated across the flowfield to the cowl. The Mach lines are allowed to cross and fold over, simulating the occurrence of embedded oblique shock waves. This procedure is continued until the entire cowl and centerbody wall pressure distributions have been determined. Figure 9 illustrates the left-running Mach lines in the supersonic flowfield of nozzle N1 as an example of the MOC code solution. Note the occurrence of a mild right-running oblique shock wave near the end of the cowl in this nozzle.

An alternative to the throat flowfield defined by the VNAP code is to simply assume the geometry of
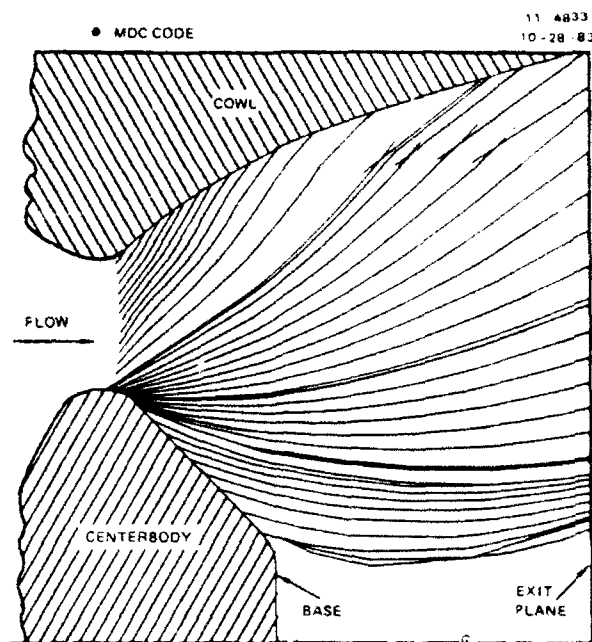
● MDC CODE

COWL

FLOW

CENTERBODY

BASE

EXIT PLANE

Fig. 9 Left-running Mach lines for nozzle N1.

○ MEASURED

UNIFORM IVL

VNAP IVL

COWL SHOULDER

END OF COWL

AXIAL STATION – INCHES

Fig. 10 Cowl pressures for nozzle N1.

a slightly supersonic, constant Mach number line that spans the nozzle throat. This uniform IVL is then treated in the same manner as the VNAP-defined IVL for throat thrust calculations and MOC code usage. As will be shown, this alternative procedure provides good results if the throat flowfield is reasonably uniform.

The predicted and measured cowl pressure distributions are presented in Figure 10. The predicted pressures are presented for two IVL's: the IVL determined from the VNAP code and a uniform IVL with a constant Mach number of 1.02. The two predicted pressure distributions are reasonably close, indicating that the subsonic/transonic flowfield for this nozzle does not differ greatly from a uniform flowfield. The Mach number distributions previously presented in Figure 8 support that conclusion. The measured pressure distribution agrees well with the predicted results except in the region just downstream of the cowl shoulder where the predicted pressure rise is more rapid than the measured rise.

The cowl and centerbody base thrusts are computed by assuming that a uniform pressure acts over these base areas. Base pressures must be estimated from empirical correlations. In the present investigation, the cowl base pressure was equated to the ambient pressure. Based on a limited amount of experimental data, the centerbody base pressure was assumed to be five percent of the nozzle chamber stagnation pressure.

The predicted and measured values of the nozzle pressure ratio efficiency are presented in Figure 11. (Nozzle efficiency definitions are discussed in the Appendix of this paper.) The observed trend of measured efficiency as a function of nozzle pressure ratio follows the predicted trend very closely. The magnitude of the predicted efficiency is approximately one percent less than the measured
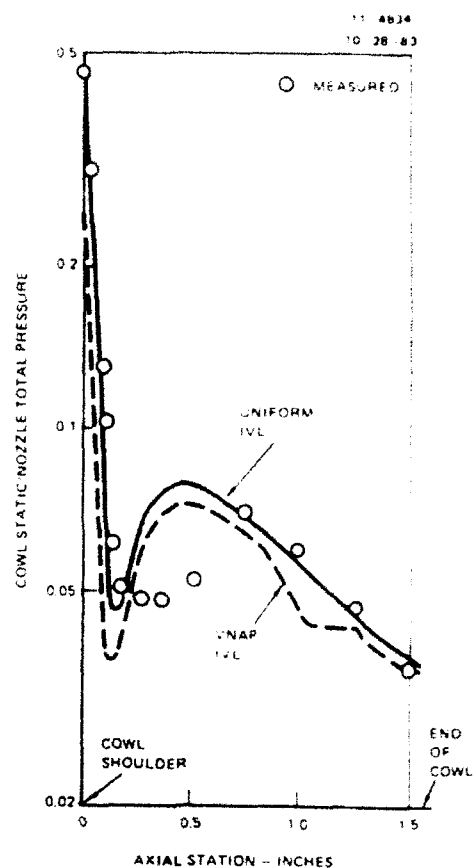
○ – MEASURED

UNIFORM IVL

VNAP IVL

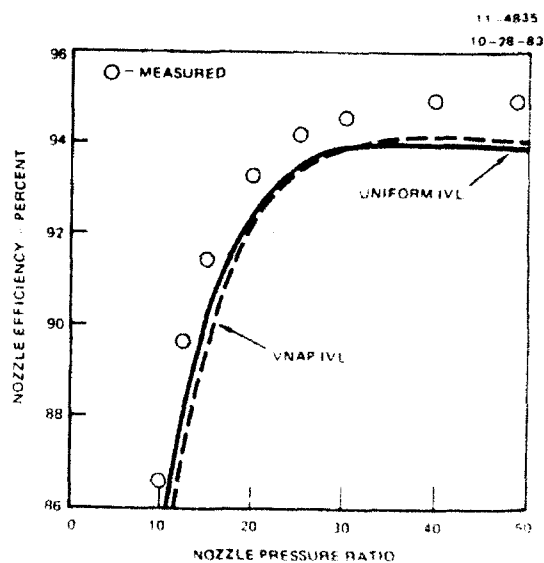NOZZLE EFFICIENCY – PERCENT

NOZZLE PRESSURE RATIO

Fig. 11 Efficiency comparison for nozzle N1.

efficiency, which is excellent agreement. These
results demonstrate that the performance prediction
methodology developed during this investigation is
capable of accurately predicting the flowfield and
performance of annular nozzles.

Results

The results of the flowfield analysis, perfor-
mance prediction and experimental testing of three
other annular nozzle configurations are presented
in this section. These three nozzles, which have
their centerbodies located downstream, upstream and
in the throat plane, exercise the capabilities of
the methodology and illustrate its strengths and
weaknesses.

Nozzle N2

Figure 12 depicts the geometry of nozzle N2.
The nozzle has an axisymmetric cowl consisting of a
cylindrical upstream section, a conical-circular
arc shoulder section and a contoured downstream
section. The axisymmetric centerbody has a cylin-
drical upstream support section, a conical initial
section, a circular arc shoulder section, a conical
section downstream of the shoulder and a flat aft
facing base. Note that the centerbody shoulder is
downstream of the cowl shoulder.

Fig. 13 Mach number distribution for nozzle N2.

Fig. 12 Geometry of nozzle N2.

Figure 13 presents the Mach number distribu-
tion obtained by the VNAP code for this nozzle. The
flowfield is highly distorted in the transonic
region. The Mach number contours show a rapid
expansion around the cowl shoulder, with the Mach
number reaching values larger than 1.5. This highly
supersonic region is followed by a rapid compression
which causes the flow to go subsonic on the cowl.
This compression is caused by the rapid inward
turning of the cowl contour, coupled with the
considerable radially outward momentum in the tran-
sonic flowfield.

The VNAP code solves the Navier-Stokes equa-
tions for unsteady flow using MacCormack's finite
difference scheme and the steady-state flowfield is
obtained as the asymptotic solution at large time.
The VNAP code uses this scheme to obtain the
flowfield solution on lines which are perpendicular
to the axis of the nozzle. This approach works best
if the finite difference grid is well matched to the

physical geometry to be analyzed. That is, accurate
flowfield solutions are obtained if the flow stream-
lines are nearly perpendicular to the solution
lines. However, if large radial flows are present,
the flow streamlines cross the solution lines at
small angles and large errors in flow properties can
occur. Therefore, the throat thrust calculated for
the VNAP-defined IVL for nozzle N2 may be in
considerable error.

When the VNAP-defined IVL for nozzle N2 is
employed in the MOC code to determine the supersonic
flowfield, the flow goes subsonic on the cowl and
the code aborts at an axial location corresponding
to the subsonic pocket.

Attempts were made to obtain a supersonic
solution by starting the MOC code with a uniform IVL
across the nozzle geometric throat (i.e., the conic
section defined by the line connecting the center of
curvature of the cowl shoulder and the center of
curvature of the centerbody shoulder) for Mach
numbers of 1.01 and 1.02. Both attempts resulted in
MOC code aborts due to the computed flow becoming
subsonic on the cowl. However, for a Mach number of
1.03, the flow remained supersonic and a flowfield
calculation was obtained.

Figure 14 presents the pressure distributions
on the cowl obtained from the MOC solution for the
uniform IVL and the VNAP IVL. For the uniform IVL
solution, the initial expansion is followed imme-
diately by a strong compression which decelerates
the flow to only a slightly supersonic Mach number.
Downstream of the nearly constant pressure region,
the pressure drops smoothly. For the VNAP IVL, the
flow initially expands to a lower pressure because
of the effects of the upstream geometry. The
recompression then results in a subsonic flow region
that causes the MOC code to abort. The experimental
measurements of static pressure on the cowl, also
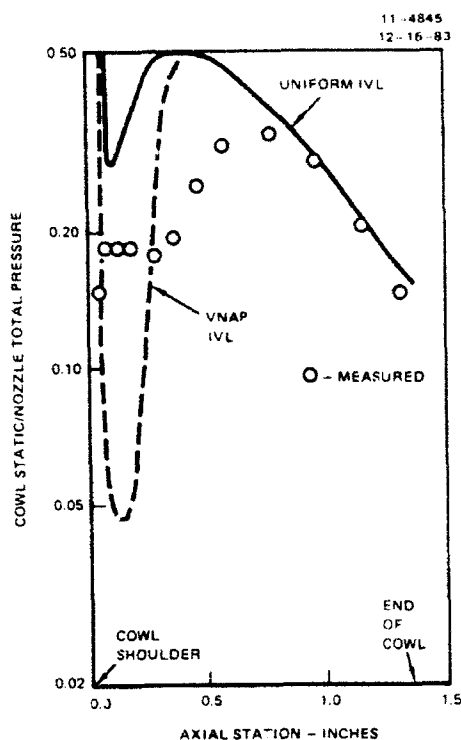presented in Figure 14, indicate that the initial

6

Fig. 14 Cowl pressures for nozzle N2.

expansion is more rapid than the uniform IVL solution predicts, but not as rapid as the VNAP IVL solution indicates. The recompression is clearly indicated, but the flow apparently remains supersonic. Note that the computed and measured pressures agree well at more downstream cowl locations.

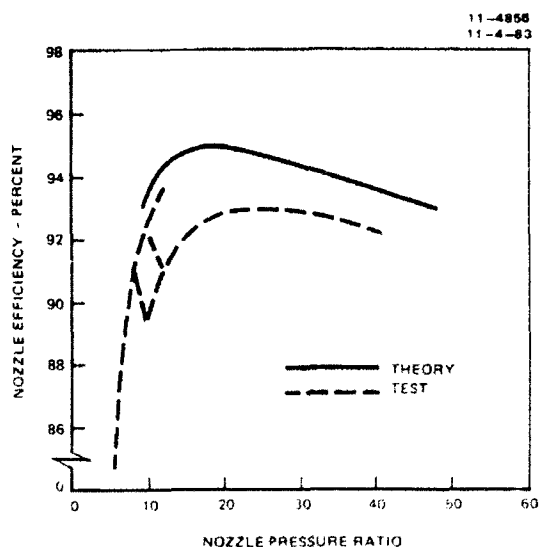The predicted and measured nozzle efficiencies for nozzle N2 are compared in Figure 15. The dual

Fig. 15 Efficiency comparison for nozzle N2.

values of measured efficiencies at lower pressure ratios are due to centerbody wake structure changes which were determined by exit plane pitot pressure surveys not discussed in this paper. At higher pressure ratios, the predicted efficiencies are approximately 2 percent higher than the measured values. This difference could be anticipated since the predicted cowl pressures (Figure 14) are generally higher than the measured pressures. The inability to more accurately analyze the flowfield is disappointing, especially since the predicted presence of the high pressure region suggests that this type of nozzle could be modified to a higher performing design. This inadequacy in predictive capability is identified as a major deficiency in the state-of-the-art of nozzle flowfield analysis.

Nozzle N3

Figure 16 depicts the geometry of nozzle N3. The nozzle has an axisymmetric cowl consisting of a cylindrical upstream section, a conical-circular arc shoulder section and a conical downstream section. The axisymmetric centerbody has a cylindrical upstream support section, a conical initial section, a circular arc shoulder section, a contoured section downstream of the shoulder and a flat aft facing base. Like nozzle N1, the shoulders of the centerbody and cowl are at the same axial station.
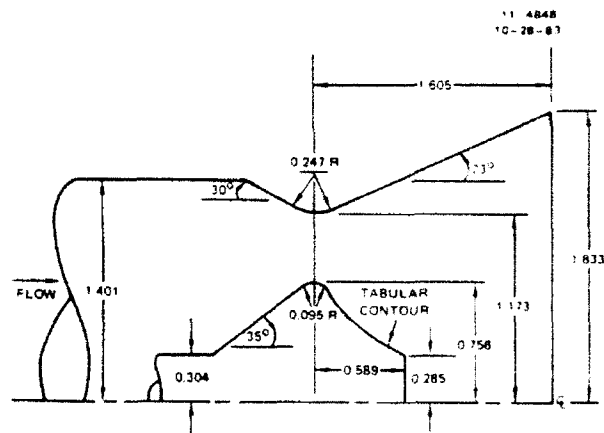
Fig. 16 Geometry of nozzle N3

The Mach number contours and Mach lines obtained by the VNAP and MOC codes are not presented since they are very similar to those previously shown in Figures 8 and 9 for nozzle N1. Figure 17 compares experimental and predicted pressure distributions on the cowl for both the uniform IVL and the VNAP IVL solutions with the MOC code. The predicted pressure distributions are almost identical and compare very well with the measured pressures for higher pressure ratios. However, as shown in Figure 17, the measured pressures at lower pressure ratios are higher than the predicted values. This difference is attributed to flow separation from the cowl. This inability to predict flow separation and compute the resulting flowfield is another major deficiency in state-of-the-art nozzle flowfield analysis.

Figure 18 compares the measured and predicted nozzle efficiencies for nozzle N3. Surprisingly, the predicted values are less than the measured efficiencies, but the agreement is excellent at
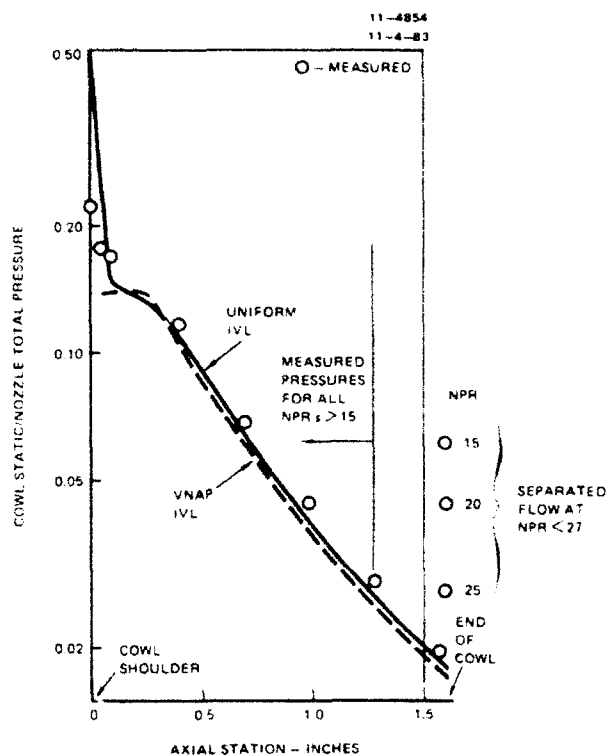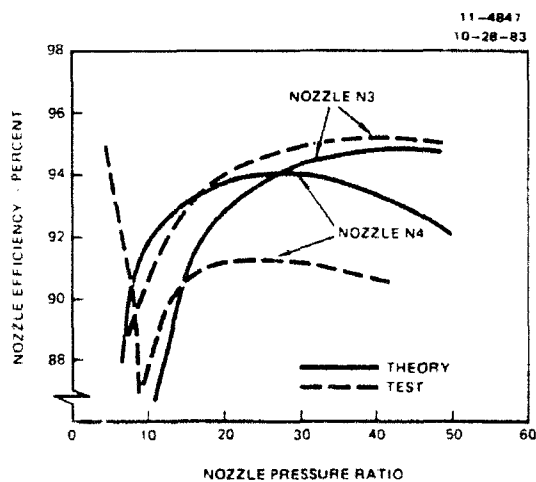
Fig. 17 Cowl pressures for nozzle N3.

Fig. 18 Efficiency comparison for nozzles N3 and N4.

higher nozzle pressure ratios. The increased difference between the measured and predicted efficiencies at lower nozzle pressure ratios merely reflects the previously mentioned flow separation phenomena.

Nozzle N4

Nozzle N4 is a rearrangement of nozzle N3 model components which locates the centerbody shoulder upstream of the cowl shoulder. This configuration completes the annular nozzle design options noted in

Figure 1. The resulting geometry for nozzle N4 is illustrated in Figure 19.
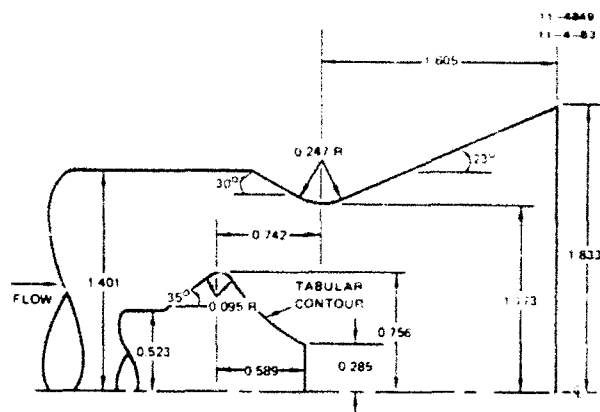
Fig. 19 Geometry of nozzle N4.

The transonic Mach number distribution obtained from the VNAP code is presented in Figure 20 and depicts a highly distorted flowfield. A region of locally supersonic flow occurs at the centerbody shoulder. The flow downstream of this region recompresses and remains subsonic all the way to the nozzle axis.
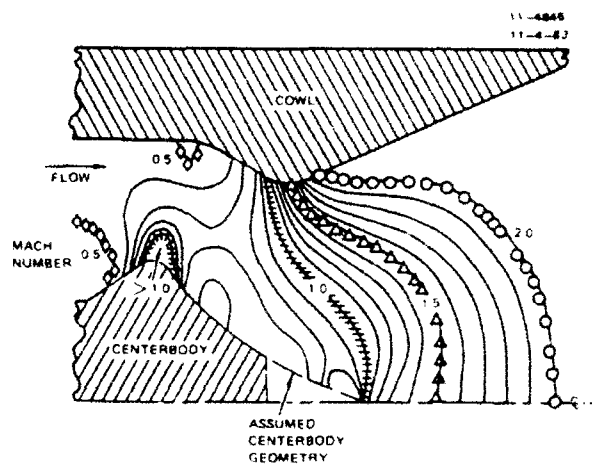
Fig. 20 Mach number distribution for nozzle N4.

Based on simple one-dimensional isentropic flow theory[7], it was assumed that the flow would choke at the minimum geometric flow area. This area is a conic surface defined by a line connecting the center of curvature of the cowl shoulder with the edge of the base. Since it was necessary to assume an extension to the centerbody for the VNAP code analysis, it was hypothesized that the assumed extension geometry influenced the results. Several different centerbody extension contours were evaluated in an attempt to obtain supersonic flow on the centerbody or its extension. However, with the exception of the previously mentioned supersonic pocket at the shoulder, the flow remained subsonic all the way to the nozzle axis for reasonable extension geometries.

8

A slightly supersonic IVL was selected from the VNAP code results and used to start the MOC code solution of the supersonic flowfield. The predicted pressure distribution on the cowl is compared with the measured pressures in Figure 21. The predicted pressures in the supersonic region downstream of the cowl shoulder do not show the degree of expansion indicated by the experimental values.
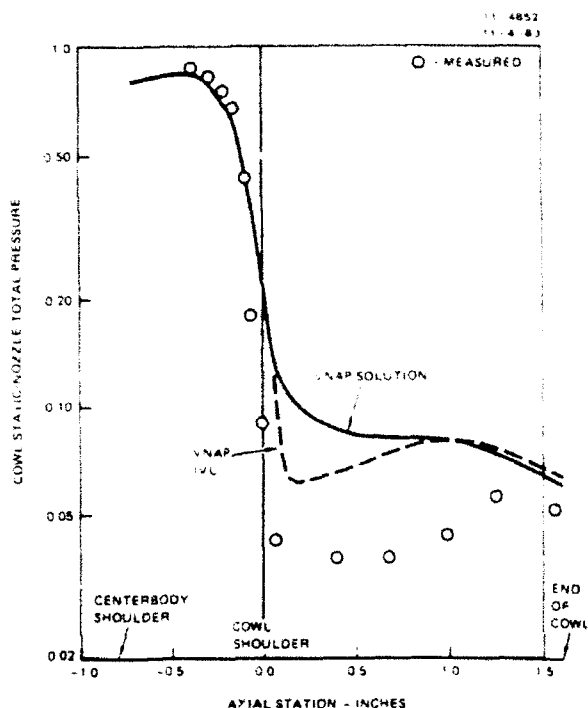

Fig. 21 Cowl pressures for nozzle N4.

Attempts were made to start the MOC code solution with a uniform IVL corresponding to the previously mentioned minimum flow area. These were unsuccessful due to the computed flow becoming subsonic. As an alternative, the VNAP code was then used to obtain a solution for the entire nozzle flowfield. Figure 21 shows that the pressures predicted by this VNAP solution agree very well with the measured values in the subsonic region upstream of the cowl shoulder. However, in the supersonic flow region downstream of the shoulder, the agreement is poorer than the predictions obtained with the MOC code using the VNAP IVL.

Figure 18 compares the measured and predicted nozzle efficiencies for nozzle N4.   The discontinuity in the measured efficiency curve near a pressure ratio of 8:1 is due to flow separation. At higher pressure ratios, the predicted efficiencies are approximately 3 percent larger than measured. This is attributed to the mismatch between the computed and measured cowl pressure distribution, as previously discussed. This difference indicates that a considerable improvement could be made in the analysis capability for this type of annular nozzle.

Nozzle Efficiency Comparison

Figure 22 compares the measured efficiencies of these four annular nozzles and the reference
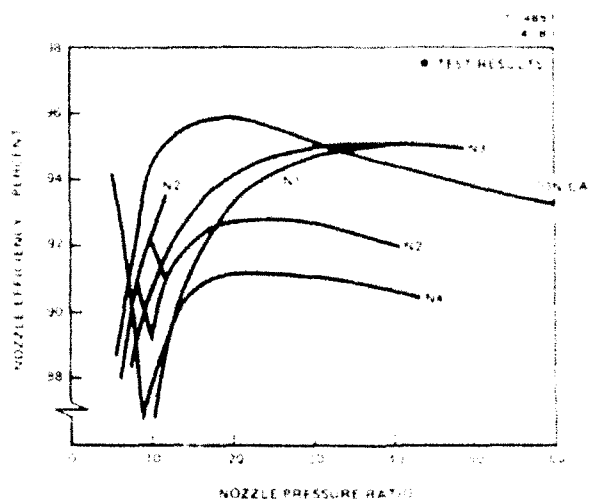
Fig. 22 Nozzle efficiency comparison.

conical nozzle. As shown, the measured efficiencies of nozzles N2 and N4 are considerably lower than those of the conical nozzle. However, the measured efficiencies of nozzles N1 and N3 indicate that they could be competitive with the conical nozzle in some applications.

Design Improvement Study

One of the primary benefits of detailed analysis of nozzle flowfields is to identify means for performance improvements. The analysis provides an increased understanding of the flowfield, from which design changes for improved performance may be proposed. Analysis also provides an inexpensive alternative to experimental comparisons of proposed design variants. As an example of such an analysis application, this section summarizes a limited study to improve the performance of nozzle N3 through small changes to the supersonic contours of the cowl and centerbody. Nozzle N3 was selected since it exhibited good predicted performance and a high degree of confidence exists in the analytical methods for this configuration. The subsonic contour of the nozzle was not altered in this study and all computations were made using the MOC code. A uniform IVL with a Mach number of 1.02 at the minimum geometric area was used to start the MOC code solution.

The effects of three design changes were investigated. They included:
(a) Replacing the aft contoured centerbody surface with a conical surface.
(b) Replacing the conical cowl with a parabolic cowl and
(c) Inserting a short cylindrical section into the centerbody just downstream of the shoulder.

The predicted results of these design changes were:
(a) Replacing the aft contoured section of the centerbody with a conical section would result in a small performance decrease.

9

(b) Contouring the cowl boundary would result
in a slight performance increase (about
0.2 percent).

(c) Adding a short cylindrical section to the
centerbody would result in a modest per-
formance increase (about 0.8 percent).

The latter approach was selected for testing
since it offered the greater potential for perfor-
mance improvement. This nozzle is denoted as N5 and
is depicted in Figure 23. The measured thrust
efficiencies for nozzle N5 and those for the refer-
ence nozzle N3 are compared in Figure 24. This
comparison verifies the predicted performance in-
crease and confirms that analytical prediction
techniques can be used to assess design changes for
performance improvements.
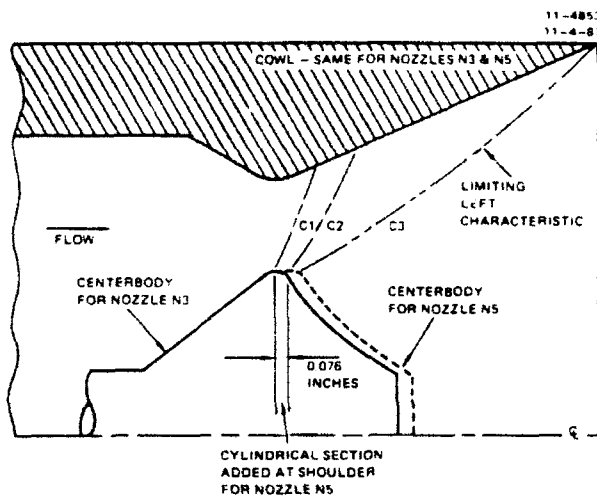
Fig. 23 Geometry of nozzle N5.
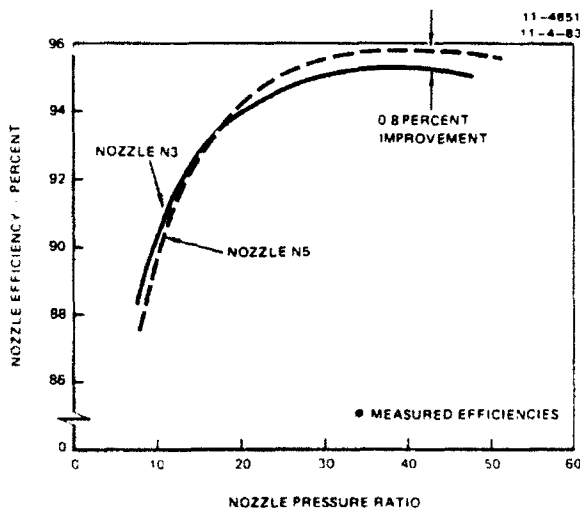
Fig. 24 Efficiency improvement with
centerbody modification.

The payoff in adding the cylindrical section to
the centerbody can be explained in terms of cowl
pressures by observing the characteristic wave

pattern, also illustrated in Figure 23. The pres-
sure distribution on the cowl is primarily deter-
mined by expansion waves emanating from the center-
body surface just downstream of Characteristic C1,
which originates at the intersection of the center-
body and the IVL. These strong expansion waves,
represented by Characteristic C2 in Figure 23, are
generated by the rapid turning of the flow around
the centerbody shoulder and cause a rapid decrease
in the pressure on the cowl. Adding a short
cylindrical section to the shoulder of the center-
body delays the turning of the flow and thus
translates the attendant pressure decrease on the
cowl further downstream. Further study of the
characteristic pattern in Figure 23 also reveals the
limiting length of the cylindrical section to
achieve performance benefits. Characteristic C3,
which intersects the end of the cowl, emanates from
the centerbody at a flow angle of approximately 15
degrees. Thus, changes to the centerbody downstream
of this point have no effect on the cowl pressure.
Any other features of the flow, specifically the
subsonic-transonic flowfield and the pressure dis-
tribution on the centerbody, should not be signifi-
cantly altered by this modification.

Summary and Conclusions

The analytical methods described in this paper
are very accurate for conventional converging-
diverging nozzles and are reasonably accurate for
annular nozzles if the radial velocity components in
the transonic region are small. The analytical
methods provide valuable quantitative information
that can be effectively used to understand the
flowfield and generate ideas for design improve-
ment. Furthermore, the methods are sufficiently
accurate that the effects of small differences in
designs can be accurately evaluated, thus reducing
the amount of experimental work required to optimize
a given design concept.

However, there are some deficiencies in the
analytical capability for some annular nozzle flow-
fields. These include inadequate transonic flow
analysis capability for flows with large radial
velocity components, inability to treat strong
shock waves (particularly when the shock waves
produce subsonic pockets in the supersonic flow-
field), very poor base pressure prediction methods
and inability to predict and calculate separated
flows. Future improvements in these areas would
enhance the analytical capability for annular noz-
zles.

Appendix
Nozzle Efficiency Definitions

Due to the importance of nozzle thrust on
propulsion system performance, a consistent nozzle
efficiency definition must be employed when compar-
ing the performance of different nozzle designs.
Since definitions of nozzle efficiency in the lit-
erature differ, the objective of this appendix is to
present a clear exposition of the various efficiency
definitions, to carefully define the various param-
eters that enter into these definitions and to
recommend a consistent procedure for the propulsive
nozzle efficiency definitions so that meaningful
comparisons can be made between various nozzles.

Three different nozzle efficiencies can be
defined. They are:

1. η_I--the internal efficiency, which compares the actual internal performance of the nozzle (i.e., vacuum performance) to the ideal internal performance of the nozzle.

2. η_{AR}--the area ratio efficiency, which compares the actual performance of the nozzle operating in an atmospheric pressure environment to the ideal performance of the nozzle operating in the same environment.

3. η_{PR}--the pressure ratio efficiency, which compares the actual performance of the nozzle operating in an atmospheric pressure environment to the ideal performance of an adapted nozzle with optimum expansion operating in the same environment.

The effect of the atmospheric pressure environment on performance is determined by the nozzle pressure ratio (NPR), which is defined as:

$$NPR = P_0/P_a \qquad (A-1)$$

where P_0 is the nozzle stagnation pressure and P_a is the ambient pressure.

Each of the three nozzle efficiency definitions has some merit. The internal efficiency measures the thermodynamic efficiency of the internal expansion process and is independent of the nozzle pressure ratio. The area ratio efficiency includes the thrust loss due to the ambient pressure acting on the backside of the nozzle. The pressure ratio efficiency includes the loss in performance when the nozzle is not adapted for operation at a particular nozzle pressure ratio.

The reference ideal thrusts required in these efficiency definitions also require careful specification of the reference ideal choking area and the reference ideal exit area of the nozzle.

Figure A-1 illustrates the reference ideal choking area A*. It is the area required to pass the actual mass flow rate and is smaller than the geometric minimum (throat) area A_t. Those two areas are related by the nozzle discharge coefficient C_D, which is defined as:

$$C_D = A^*/A_t = \dot{m}_{act}/\dot{m}_{ref} \qquad (A-2)$$

where $\dot{m}_{act}$ is the actual mass flow rate and $\dot{m}_{ref}$ is the mass flow rate corresponding to steady one-dimensional isentropic choked flow at the geometric throat area.
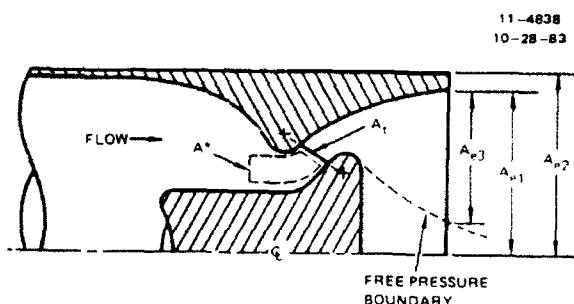
For DeLaval nozzles, the geometric throat area is defined as the planar area at the nozzle minimum cross section and values of discharge coefficient are quite close to unity. For unconventional nozzles, the choice of geometric throat area is less obvious and values of discharge coefficient may differ considerably from unity. In fact, the determination of the geometric minimum area for annular nozzles such as discussed in this paper may be quite difficult.

The actual mass flow rate may be determined experimentally, predicted analytically or determined from empirical discharge coefficient correlations. In this study, reference mass flow rate was determined using conventional steady one-dimensional isentropic nozzle flow theory[ ] and actual mass flow rate was predicted using the Viscous Nozzle Analysis Program (VNAP) code[4].

Figure A-1 also illustrates the reference ideal exit area of the nozzle. It can be defined in several ways, for example:
(1) the nozzle maximum internal area A_{e1}, or
(2) the nozzle maximum internal area plus the cowl base area A_{e2}.
Since the flow always separates from the centerbody aft face and forms a free-pressure boundary, the reference ideal area could be defined as either of the preceding areas minus the area occupied by the separation region, for example A_{e3} in Figure A-1. This choice has some merit from a fluid dynamic point of view for annular nozzles, but it is impractical since the size of the separation region is difficult to determine. In the present study, the reference ideal exit area of the nozzle is defined as A_{e1} in Figure A-1.

Once the reference ideal choking area and the reference ideal exit area have been specified, the reference ideal thrust for internal efficiency and area ratio efficiency can be computed using conventional steady one-dimensional isentropic nozzle flow theory. The reference ideal thrust for pressure ratio efficiency can be computed for a specified value of nozzle pressure ratio by the same techniques.

Figure A-2 presents the three nozzle efficiencies as a function of nozzle pressure ratio for a nozzle having a reference ideal area ratio of 3:1. (This corresponds to an adapted pressure ratio of approximately 20:1 for a gas with a specific heat ratio of 1.30.) The assumed internal efficiency is 0.97 and the assumed discharge coefficient is 0.94. The area ratio efficiency and the pressure ratio efficiency have been computed from conventional steady one-dimensional nozzle flow theory and the assumed values of internal efficiency and discharge coefficient. The area ratio efficiency shows the loss in performance of the particular nozzle due to the atmospheric pressure, while the pressure ratio efficiency shows the loss in performance due to improper matching of the design area ratio with the operating pressure ratio. The two efficiencies are equal only at the design area ratio.

The pressure ratio efficiency is the most meaningful for comparing different nozzle designs operating over a range of nozzle performance ratios. Consequently, that efficiency was employed in the present investigation.
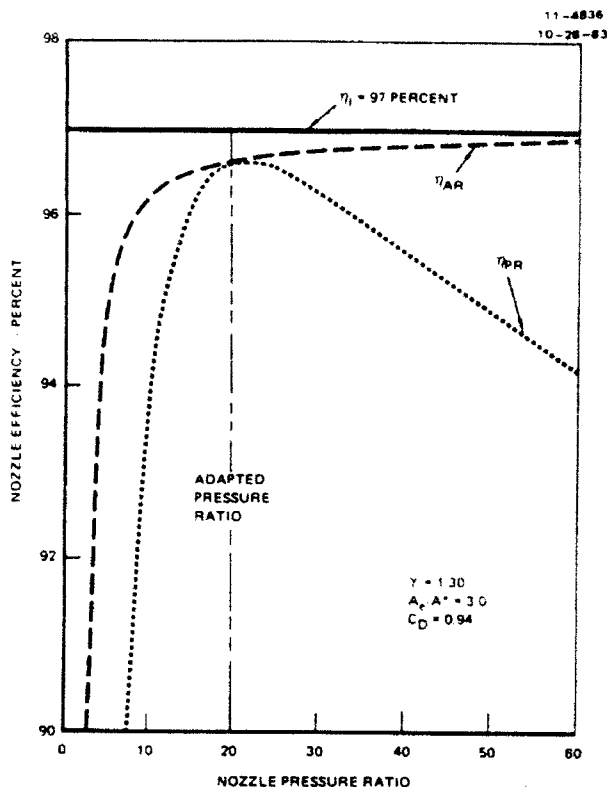

11-4838
10-28-83

FREE PRESSURE BOUNDARY

Fig. A-1 Reference areas for an annular nozzle.

Fig. A-2 Comparison of nozzle efficiency
definitions.

References

1. Rao, G.V.R., "Exhaust Nozzle Contour for Opti-
    mum Thrust," Jet Propulsion, Volume 28, No. 6,
    pp. 377-382, June 1958.

2. Schorr, C.J. and McKenna, R.F., "Constant
    Chamber Pressure Throttling of an Expansion-
    Deflection Nozzle," AIAA Paper 69-435, June
    1969.

3. Zucrow, M.J. and Hoffman, J.D., Gas Dynamics,
    Vol. 1, Chapter 10, John Wiley and Sons, New
    York, 1975.

4. Cline, M.C., "VNAP: A Computer Program for
    Computation of Two-Dimensional, Time Dependent
    Compressible, Viscous, Internal Flow," Report
    LA-7326, Los Alamos Scientific Laboratory. Los
    Alamos, NM, November 1978.

5. Thompson, H.D., "A Method of Characteristics
    Program for Computing Annular Nozzle Flow-
    fields," Report ME-TSPC-83-05, Thermal Sci-
    ences and Propulsion Center, Purdue Univer-
    sity, West Lafayette, IN, June 1983.

6. MacCormack, R.W., "The Effect of Viscosity in
    Hypervelocity Impact Cratering," AIAA Paper
    69-354, April 1969.

7. Zucrow, M.J. and Hoffman, J.D., Gas Dynamics,
    Vol. 1, Chapter 4, John Wiley and Sons, New
    York, 1975.

AIAA'85

AIAA-85-0364
An Analytical Investigation of the Effects
of Swirl on Annular Propulsive Nozzles
B. T. Kornblum, H. D. Thompson, and J. D.
Hoffman, Purdue Univ., West Lafayette, IN

AIAA 23rd Aerospace Sciences Meeting

January 14-17, 1985/Reno, Nevada

AN ANALYTICAL INVESTIGATION OF THE

EFFECTS OF SWIRL ON ANNULAR PROPULSIVE NOZZLES

Barbara T. Kornblum[*]
Lawrence Livermore National Laboratory
Livermore, California 94550

and

H. Doyle Thompson[+] and Joe D. Hoffman[++]
Purdue University
West Lafayette, Indiana 47907

Abstract

An analytical perfomance prediction methodology for annular propulsive nozzles with swirl introduced in the combustor upstream of the nozzle is presented. The application of that methodology to a specific nozzle design for a free vortex swirl distribution is discussed. Discharge coefficients, specific impulses, and wall pressure distributions are presented. These numerical studies show that the discharge coefficient and the thrust decrease as the amount of swirl increases, but that the specific impulse is essentially uninfluenced by the swirl. This methodology will enable nozzle designers to account for the effects of swirl in nozzle design.

Nomenclature

a	speed of sound
C_1-C_4	constants specifying tangential velocity distributions
F	thrust
$\dot{m}$	mass flow rate
M	Mach number
P	static pressure
P_o	stagnation pressure
R	gas constant
S	swirl number
t	time
T	static temperature
T_o	stagnation temperature
u	axial velocity component
v	radial velocity component
w	tangential velocity component
x,y	axial and radial coordinate, respectively
Y_1	inner radius of the annular flow geometry
Y_2	outer radius of the annular flow geometry
γ	specific heat ratio
ρ	density
θ	tangential coordinate

---

[*] Graduate Student in Mechanical Engineering. Presently with Lawrence Livermore Laboratory.

[+] Professor of Mechanical Engineering. Associate Fellow AIAA.

[++] Professor of Mechanical Engineering. Member AIAA.

Subscripts

A to F	denotes geometric stations
B,C,P,IVL	denote base, cowl, plug, and initial-value line
t,x,y	denotes partial differentiation

Introduction

Recent studies indicate that the introduction of swirl ahead of the combustor in axisymmetric dump combustors can have very beneficial effects on the combustion process. Buckley, Craig, Davis and Schwartzkopf[1] found that swirl both reduced the reattachment length of the combustor flowfield (thereby reducing the overall combustor length needed for good performance), and helped eliminate destructive very low frequency instabilities. They further concluded that (in the range of swirl intensities of their study) "losses in thrust due to residual swirl, at least to the sonic point of the nozzle, are negligible."

Scharrer and Lilley[2] made five-hole pitot probe measurements of the effects of swirl in simulated dump combustors followed by a nozzle. They observed a significant interaction between the swirling flowfield in the simulated combustor and the nozzle flowfield. Their major objective, however, was the measurement of the confined turbulent flow in the simulated combustor, not the nozzle flowfield. Consequently, their nozzles were simply used as downstream blockage components. Both nozzles used in their studies were conventional converging nozzles without centerbodies.

Conley, Hoffman and Thompson[3] presented an analytical and experimental investigation of the performance of annular propulsive nozzles without swirl. The present work is an extension of the performance prediction methodology developed by Conley, Hoffman, and Thompson to include the effects of swirl introduced in the combustor on the performance of annular propulsive nozzles.

A similar study performed by Dutton[4] shows trends similar to the results obtained in the present investigation for conventional convergent-divergent nozzles

1

without centerbodies. The present investigation is concerned with convergent-divergent nozzles with centerbodies.

The objective of the present work was to analytically investigate the effect of swirl on the transonic and supersonic flowfields in annular propulsive nozzles, and to determine the effects of swirl on mass flow rate, thrust, and specific impulse.

Performance Prediction Methodology

Geometric Model

The geometric model considered in this investigation is illustrated in Fig. 1. Air enters at Station A and flows through a swirler where tangential momentum is transferred to the air to give the desired tangential velocity distribution at Station B. Station B is followed by a sudden expansion dump into the combustor inlet at Station C. Combustion takes place between Stations C and D, where the stagnation temperature T_o rises corresponding to the amount of fuel added and the stagnation pressure P_o descreases slightly due to friction, mixing, and heat addition. The combustion products accelerate in the nozzle to the choked condition at the nozzle throat, Station E, after which the flow continues to accelerate supersonically from Station E to Station F.

Fig. 1. Geometric model.

The concern in the present study was the effect of swirl introduced in the swirler on the performance of the nozzle (i.e., mass flow rate, thrust, and specific impulse). Consequently, the swirler, the sudden expansion dump, and the combustor are not modeled in detail in the present analysis. Emphasis is placed on the nozzle flowfield. Even so, some attention must be given to the swirler, since it is the source of the swirl in the nozzle flowfield.

Swirler

The swirler is a set of axial flow guide vanes that imparts the desired tangential velocity distribution to the

air as it passes through the swirler. The design of the swirler and the interaction of the swirl with the combustion process are of paramount importance in an actual system design. In the present study of the effects of swirl on nozzle performance, a tangential velocity distribution representative of what might be produced by a swirler and a combustor is simply assumed to exist at the nozzle inlet.

Buckely, Craig, Davis, and Schwartzkopf[1] experimentally investigated four types of tangential velocity distributions at the swirler exit. They are:

Constant angle: $w = C_1$ (1)

Forced vortex: $w = C_2 y$ (2)

Free vortex: $w = C_3/y$ (3)

Rankine vortex: $w = (C_4/y)[1-exp(-y^2/Y_2^2)]$ (4)

where w is the tangential velocity, y is the radial location, Y_2 is the outer radius of the swirler, and C_1 to C_4 are constants specified to achieve the desired tangential velocity distribution. In order to provide a basis for comparison of different swirlers, a swirl number S is employed, which is defined as

$$S = \frac{\int_{Y_1}^{Y_2} uwy^2 dy}{Y_2 \int_{Y_1}^{Y_2} u^2 y dy} \quad (5)$$

The only tangential velocity distribution considered in the present study was the free vortex distribution given by Eq. (3). A centerbody exists throughout the flowfield, so the singularity associated with the core of a free vortex does not occur in this flowfield. For a free vortex, $yw = C_3$, so that at a uniform flow section where the radial velocity $v = 0$ and the axial velocity u is uniform, Eq. (5) simplifies to

$$S = \frac{C_3}{uY_2} \quad (6)$$

Consequently, the swirl number S is a simple function of the geometry (i.e., Y_2) and the axial velocity u. For a given value of C_3 at the nozzle inlet, Station D, the swirl number S_D can be calculated. Thus,

$$S_D = \frac{C_3}{u_D Y_{2D}} \quad (7)$$

2

The corresponding values of swirl number at the combustor inlet S_C, swirler exit S_B, and nozzle throat S_E can be estimated from the known value of S_D and Eq. (6). The major process occuring between Stations C and D is the increase in stagnation temperature T_o due to combustion. For a Rayleigh line flow (i.e., heat addition at constant area) in the absence of swirl, it can be shown that

$$\frac{u_D}{u_C} = \frac{RT_{oD} + \frac{\gamma+1}{2\gamma} u_D^2}{RT_{oC} + \frac{\gamma+1}{2\gamma} u_C^2} \qquad (8)$$

Thus, for known values of u_D, T_{oD}, and T_{oC}, u_C can be calculated, so that

$$\frac{S_D}{S_C} = \frac{C_3/u_D Y_{2D}}{C_3/u_C Y_{2D}} = \frac{u_C}{u_D} \qquad (9)$$

At the sudden expansion dump location, Y_2 changes from Y_{2B} to Y_{2C}. For constant mass flow rate $\dot{m}$, and neglecting compressibility effects, which are small, u is inversely proportional to the flow area, which is directly proportional to Y_2^2. Thus,

$$u_B = u_C (Y_{2C}/Y_{2B})^2 \qquad (10)$$

Substituting this result into Eq. (6) yields

$$\frac{S_C}{S_B} = \frac{C_3/u_C Y_{2C}}{C_3/u_B Y_{2B}} = \frac{Y_{2C}}{Y_{2B}} \qquad (11)$$

At the nozzle throat, Station E, u_E is three to five times as large as u_D, and Y_{2E} may be anywhere from 50 to 90 percent of Y_{2D}. When specific values are given, S_E can be calculated from S_D.

Consequently, for a specified value of the swirl yw at the nozzle inlet, the swirl number S_D at the nozzle inlet can be calculated. Knowing the other motor operating parameters, the values of the swirl number S can be estimated at other locations in the motor.

Performance Model

The propulsive nozzle is the thrust producing component of jet propulsion engines such as rockets, turbojets and ramjets. The function of the propulsive nozzle is to convert the random thermal energy of the gases entering the nozzle into directed kinetic energy at the nozzle exit, thus creating a thrust on the propulsive system. The expansion process must be accomplished as efficiently as possible, since the gross thrust developed by the nozzle is directly related to the nozzle exhaust velocity. For rocket engines, the gross thrust produced by the nozzle is also the net thrust. However, for airbreathing engines (turbines and ramjets), the net thrust is the difference between the nozzle gross thrust and the inlet ram drag. Consequently, all losses in nozzle gross thrust for airbreathers are magnified several times in net thrust, and it is imperative that the nozzle efficiency be as large as possible.

Figure 2 illustrates the thrust producing components of a generic annular nozzle. The nozzle thrust is composed of the thrust developed across the supersonic initial-value line F_{IVL}, the thrust developd by the pressure acting on the cowl F_C, the thrust developed by the pressure acting on the plug F_P, and the thrust acting on the plug base F_B.
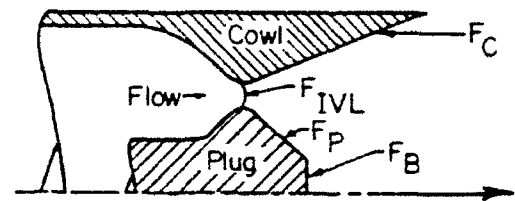

Fig. 2. Thrust producing components of an annular nozzle.

The relative magnitudes of these thrust components depend on the nozzle design. For nozzle geometric area ratios between 3 and 5, as considered in this study, the magnitude of the supersonic initial-value line thrust is approximately 80 to 85 percent of the total thrust, the cowl thrust is from 10 to 15 percent of the total thrust, and the plug and base thrusts comprise the remainder.

The supersonic initial-value line thrust F_{IVL} is given by

$$F_{IVL} = \int_{IVL} u \, dm + \int_{IVL} P \, 2\pi y \, dy \qquad (12)$$

The cowl thrust F_C is given by

$$F_C = \int_{Cowl} P \, 2\pi y \, dy \qquad (13)$$

The plug thrust F_P is given by

$$F_P = \int_{Plug} P \, 2\pi y \, dy \qquad (14)$$

3

The plug base thrust F_B is given by

$$F_B = P_B A_B \qquad (15)$$

where P_B is the average base pressure acting on the truncated plug base area A_B.

From Eqs. (12) to (15), it is seen that the flow properties across the supersonic initial-value line, the pressure distributions along the cowl and the plug, and the base pressure must be calculated to enable the calculation of the nozzle performance.

Flowfield Model

The accuracy and efficiency of nozzle performance prediction techniques are highly dependent on the flowfield model chosen to represent the actual flowfield. In the present study, the flowfield model is based on the following assumptions:

1. steady axisymmetric flow,
2. inviscid nonconducting fluid,
3. no body forces,
4. thermally and calorically perfect gas, and
5. separation and base pressures predicted from empirical correlations.

The governing equations consist of the continuity equation, the component momentum equations, the energy equation and the thermal and caloric equations of state. A detailed discussion of these equations is presented in Ref. (5).

The choice of a numerical method, or methods, to solve these governing equations is also crucial to the success of the performance prediction procedure. A subsonic/transonic solution is required to define the supersonic initial-value line thrust, while a supersonic solution is required to define the cowl, plug, and base thrusts. Experience[3] has shown that subsonic/transonic flowfields can be adequately determined from the steady state solution to finite difference time marching solutions, whereas the method of characteristics is the most accurate means for determining supersonic flowfields in nozzles. Therefore, the numerical methods selected for the performance prediction procedure in the present study are a finite difference time marching approach to define the subsonic/transonic flowfield, and a method of characteristics approach to define the supersonic flowfield.

Subsonic/Transonic Flowfield

The finite difference code developed to solve the subsonic/transonic flowfield is a modification of the VNAP (Viscous Nozzle Analysis Program) code developed by Cline[6] to include the effects of swirl. The resulting code is called SNAP (Swirling Nozzle Analysis Program).

The VNAP code was used as the subsonic/transonic flowfield prediction code for the annular nozzle performance prediction methodology developed by Conley, Hoffman, and Thompson[3]. The VNAP code solves the Navier-Stokes equations for two-dimensional (planar or axisymmetric), time dependent, compressible flow using the second-order accurate, MacCormack[7] finite difference scheme. Inviscid flowfields can be solved by setting all of the viscous terms to zero, which yields the Euler equations. An explicit artificial viscosity is included for shock wave calculations. The fluid is assumed to be a perfect gas. The steady state solution is obtained as the asymptotic solution for large time.

The computational grid employed by the VNAP code is a transformed equally spaced grid. Equally spaced lines of constant ζ normal to the x-axis comprise one of the transformed coordinates. Each vertical line segment between the plug and the cowl is divided into a number of equally spaced increments. Lines of constant η join these points. The physical grid is illustrated in Fig. 3. The transformation equations are

$$\zeta = x \quad \text{and} \quad \eta = \frac{y - y_C(x)}{y_C(x) - y_P(x)} \qquad (16)$$

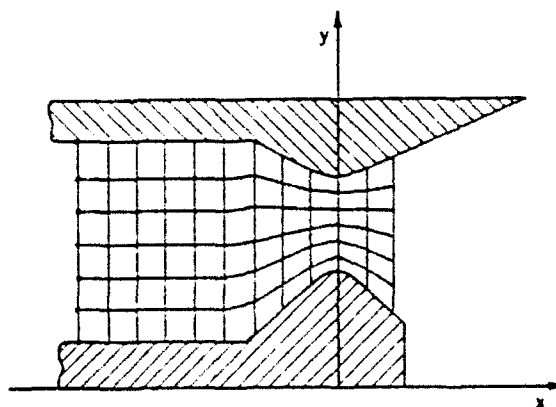where $y_C(x)$ is the cowl contour and $y_P(x)$ is the plug contour.

Fig. 3. Typical SNAP grid.

In the present investigation, the VNAP code was modified to account for the presence of swirl in the flowfield by adding the tangential momentum equation to the set of governing equations and the tangential velocity component to all the governing equations, where appropriate. Since the flowfield is axisymmetric, all derivatives with respect to the tangential direction θ are zero, even though the

tangential velocity component w is nonzero. The governing equations for this flowfield are:

$$\rho_t + u\rho_x + v\rho_y + \rho u_x + \rho v_y + \rho v/y = 0 \quad (17)$$

$$\rho u_t + \rho u u_x + \rho v u_y + P_x = 0 \quad (18)$$

$$\rho v_t + \rho u v_x + \rho v v_y + P_y - \rho w^2/y = 0 \quad (19)$$

$$w_t + u w_x + v w_y + vw/y = 0 \quad (20)$$

$$P_t + u P_x + v P_y - a^2(\rho_t + u\rho_x + v\rho_y) = 0 \quad (21)$$

where u, v, and w are the velocity components in the x, y, and θ directions, respectively. P is the pressure, ρ is the density, a is the speed of sound, and subscripts denote partial differentiation. For a perfect gas,

$$P = \rho R T \quad (22)$$

$$a^2 = \gamma P/\rho \quad (23)$$

Equation (20) can be written as

$$\frac{D(yw)}{Dt} = 0 \quad (24)$$

which is in substantial derivative form. Equation (24) states that the swirl yw remains constant on the pathlines of an unsteady flowfield and on the streamlines of a steady flowfield. Consequently, if the distribution of the swirl yw is specified at the nozzle inlet, that swirl distribution will be preserved throughout the flowfield. Thus, two modifications to VNAP were made to include the effects of swirl: (1) tracking the streamlines of the flowfield so that the values of swirl yw at the nozzle inlet can be tracked through the flowfield as the streamlines change radial position, and (2) adding the term $\rho w^2/y$ to Eq. (19), where w is computed from the known value of swirl yw along each streamline.

The initial tangential velocity distribution w(y) is specified at Station B, illustrated in Fig. 4. Station B is an upstream station ahead of the nozzle inlet. Typically, Station B is the exit of the swirler. The mass flow distribution $\dot{m}(y)$ is computed across Station B, so that the swirl yw is a known function of $\dot{m}$. This function, yw($\dot{m}$), is then used to compute the swirl yw at each point in the
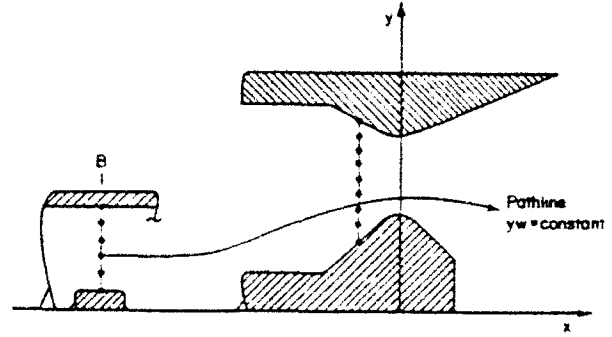

Fig. 4. Swirl specification model.

nozzle in the following manner. After each time step, the mass flow rate is integrated across the flowfield at each axial location, from the centerbody ($\dot{m} = 0$) to the nozzle wall ($\dot{m} = \dot{m}_{total}$). The fractional mass flow rate at each radial station is calculated by dividing the calculated mass flow rate at that radial station by the total mass flow rate at that axial location. The resulting fractional mass flow rate is then used to interpolate for the swirl yw at the corresponding computational grid point by quadratic interpolation of the swirl function yw($\dot{m}$) computed at Station B. The swirl velocity w is then computed by dividing the interpolated value of the swirl yw by the value of y at the computational grid point.

This procedure is consistent with the governing partial differential equations only at the steady flow limit, because actual unsteady pathlines are not tracked. Essentially, this procedure matches a normalized steady mass flow rate at the swirler exit to a normalized mass flow rate at each point in the nozzle. In an unsteady flow, these two points would not necessarily lie on the same pathline. However, at the steady flow limit, these two points do lie on the same streamline.

In a typical run, 800 to 1000 time steps are taken by the SNAP code to relax the initially assumed one-dimensional flowfield to a steady state. An initial-value line along which the projection of the Mach number in the xy plane is supersonic is then specified across the throat region. Values of the projected Mach number and flow angle along that line are determined from the SNAP flowfield by interpolation. Least squares quadratic bivariate interpolating polynomials are fit to the nine closest SNAP grid points to each initial-value line point. In this manner, a supersonic initial-value line is determined, which can be used to initiate the solution of the supersonic flowfield by the method of characteristics.

5

Supersonic Flowfield

The supersonic flowfield is calculated by the method of characteristics for steady two-dimensional flow. For steady flow, Eqs. (17) to (21) become

$$u\rho_x + v\rho_y + \rho u_x + \rho v_y + \rho v/y = 0 \quad (25)$$

$$\rho u u_x + \rho v u_y + P_x = 0 \quad (26)$$

$$\rho u v_x + \rho v v_y + P_y - \rho w^2/y = 0 \quad (27)$$

$$u w_x + v w_y + v w/y = 0 \quad (28)$$

$$u P_x + v P_y - a^2(u\rho_x + v\rho_y) = 0 \quad (29)$$

Equation (28) can be written as

$$\frac{D(yw)}{Dt} = 0 \quad (30)$$

which states that the swirl yw is constant along streamlines.

The derivation of the characteristic and compatibility equations corresponding to Eqs. (25) to (29) is a straightforward, although somewhat lengthy, procedure. The derivation is presented by Kornblum and Thompson[8]. The results are not presented here. In brief, three characteristics are determined in the xy plane: the streamline and the right- and left-running Mach lines. Three compatibility equations are determined along the streamline and one compatibility equation is determined along each Mach line. These five compatibility equations are used to solve for u, v, w, P, and ρ.

A direct marching method of characteristics procedure is employed to solve the characteristic and compatibilty equations. The solution procedure constructs the Mach line network illustrated in Fig. 5. The characteristic and compatibility equations are integrated numerically by the second-order accurate modified-Euler predictor-corrector method. The solution is initiated from the supersonic initial-value line, line TT', determined from the SNAP analysis. Left-running Mach lines are emanated from line TT', starting at point T, and continued across the flowfield until they intersect the cowl, contour TE. The last such Mach line from point T' intersects the cowl at point T". Left-running Mach lines are then originated from points on the centerbody and continued across the flowfield to intersect the nozzle wall. This procedure is
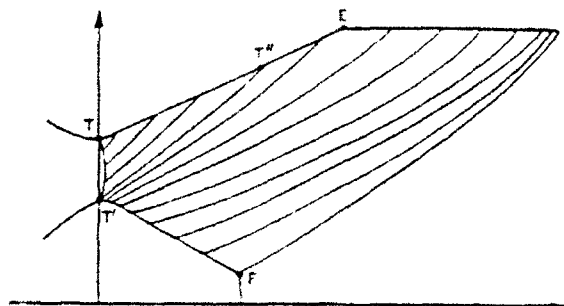

Fig. 5. Typical left-running Mach lines for supersonic annular swirling flow.

continued until the nozzle exit lip point, point E, is determined. Left-running Mach lines are then terminated at the last right-running Mach line emanating from Point E. This procedure is continued until point F, at the end of the plug is determined. The base pressure on the face of the truncated plug is computed from the following empirical correlation:

$$P_{base} = 0.846 \, P_F/M_F^{1.3} \quad (31)$$

The above procedure determines all of the data required to evaluate the thrust components illustrated in Fig. 2.

Results

Nozzle flowfields were computed for 12 cases. Figure 6 defines the flowfield geometry for all 12 cases. Only free vortex swirlers were considered. The swirl strength was characterized by the yw product, where y is the flow radius (ft), and w is the trangenital velocity component (ft/sec). Values of the swirl yw of 0, 50, 100, 150, 200, and 250 ft^2/sec were analyzed for stagnation temperatures at the nozzle inlet of 2500 R and 3500 R. The stagnation pressure was 35 psia in every case. In all cases, the specific heat ratio $\gamma = 1.40$ and the gas constant R = 53.35 (ft-lbf)/(lbm-R). The scope of the parametric study is defined in Table 1.

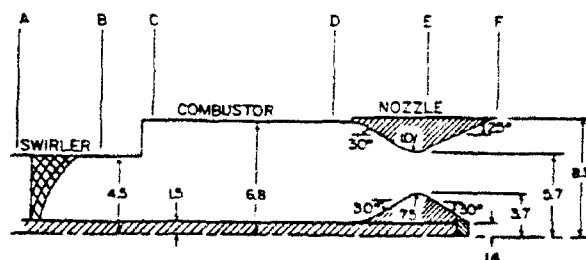Fig. 6. Nozzle geometric specification.

6

Table 1. Scope of the parametric study.

Run	Swirl yw (ft^2/sec)	T_O R
1	0	2500
2	50	2500
3	100	2500
4	150	2500
5	200	2500
6	250	2500
7	0	3500
8	50	3500
9	100	3500
10	150	3500
11	200	3500
12	250	3500

Fig. 7. Transonic Mach number distribution for Case 7.

The swirl number S defined by Eq. (5) varies with axial location in the flow-field. At the nozzle inlet (x = - 6.0 in. for the SNAP analysis), a swirl yw of 50 ft^2/sec corresponds approximately to a swirl number S = 0.14 for T_o = 2500 R, and S = 0.12 for T_o = 3500 R. The swirl number S varies approximately linearly with the swirl yw at that location, so that the range of yw values considered in this study (i.e., 0 to 250 ft^2/sec) corresponds to swirl numbers between 0 and 0.7 at the nozzle inlet. At the nozzle throat, the swirl numbers are, of course, much smaller. For the nozzle geometry considered here, the swirl numbers at the throat are about 30 percent of the values at the nozzle inlet.

The swirl number upstream of the combustor depends on the amount of heat added in the combustor, as indicated by Eqs. (8) and (9). For stagnation temperatures of approximately 1000 R entering the combustor and a swirl yw = 50 ft^2/sec, S = 0.37 for T_o = 2500 R and S = 0.44 for T_o = 3500 R. The swirl number varies approximately linearly with yw, so the range of yw values considered in this study corresponds to swirl numbers between 0 and 2.20 at the combustor inlet.

The swirl number at the swirler exit, upstream of the sudden expansion dump, depends on the geometry of the sudden expansion, as expressed by Eq. (11). For yw = 50 ft^2/sec, S = 0.24 for T_o = 2500 R at the nozzle inlet, and S = 0.29 for T_o = 3500 R at the nozzle inlet. The swirl number varies approximately linearly with yw, so the range of yw values considered in this study corresponds to swirl numbers between 0 and 1.45 at the swirler exit.

Figure 7 presents constant Mach number lines in the transonic region for Case 7 (T_o = 3500 R, yw = 0) as computed by the SNAP code. Comparisons with the constant Mach number lines for the other 11 cases show differences in the third significant figure for most quantities.
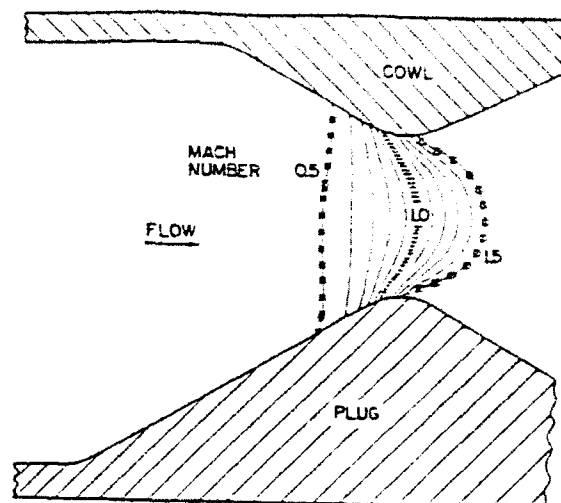
Thus, Fig. 7 is representative of the plots for all 12 cases. There are some differences, however, which are discernible in the integrated mass flow rate values tabulated in Table 2.

Figures 8 and 9 present the left-running Mach line pattern in the xy-plane for the supersonic flowfields for Cases 1 and 6, respectively. Case 1 is the no swirl case with T_o = 2500 R. Case 6, yw = 250 ft^2/sec and T_o = 2500 R, represents the largest swirl case considered in the study. In Figs. 8 and 9, the left-running Mach lines emanating from the plug surface are terminated at the right-running Mach line emanating from the end of the cowl. Comparison of Figs. 8 and 9 shows that swirl has the effect of compressing the flow on the plug surface, resulting in coalescing left-running Mach lines.
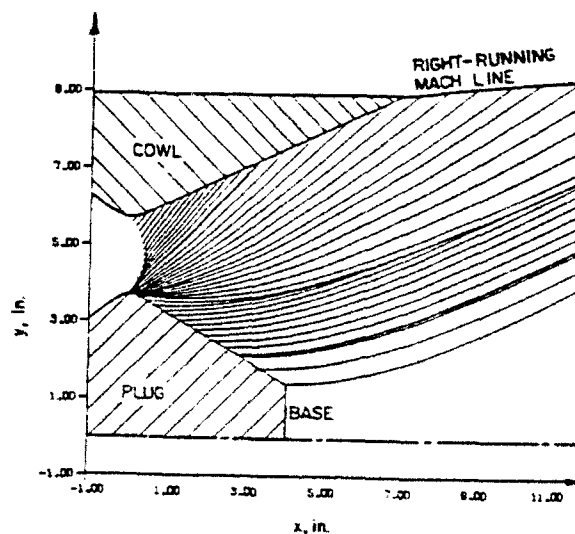

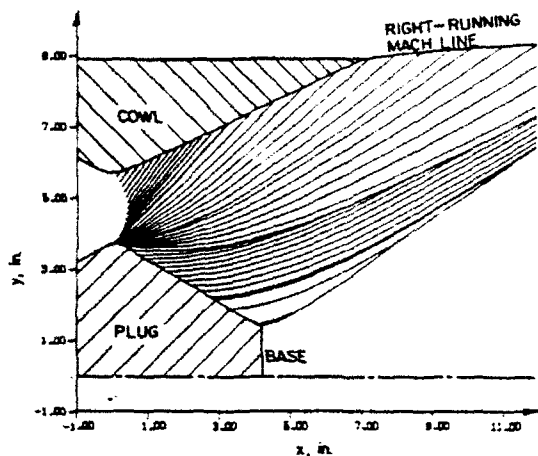Fig. 8. Left-running Mach lines for Case 1.

Fig. 9. Left-running Mach lines for Case 6.

Figure 10 is a comparison of the pressure distributions on the plug for Cases 1 and 6. There is a substantial pressure increase on the plug due to the effects of swirl. Unfortunately, the area over which the pressure increase acts is small, so the increase in thrust is only modest. The pressure distributions for the intermediate swirl intensities lie between the results of Cases 1 and 6 in a very orderly fashion.
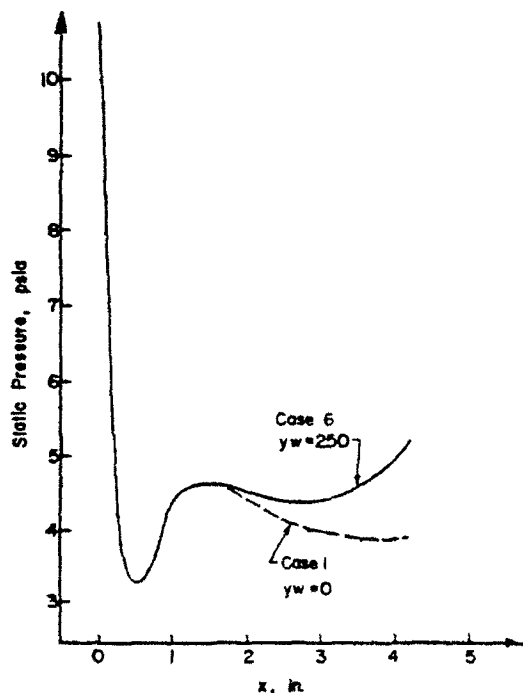
Figure 11 presents the pressure distribution on the cowl for Cases 1 and 6. The pressure distributions on the cowl surface are almost indistinguishable for all swirl values. There are some differences, however, which are discernable in the integrated thrust values tabulated in Table 2. Because the cowl projected area is much larger than the plug area, a much smaller pressure difference is required to produce distinguishable differences in the integrated thrust values on the cowl.
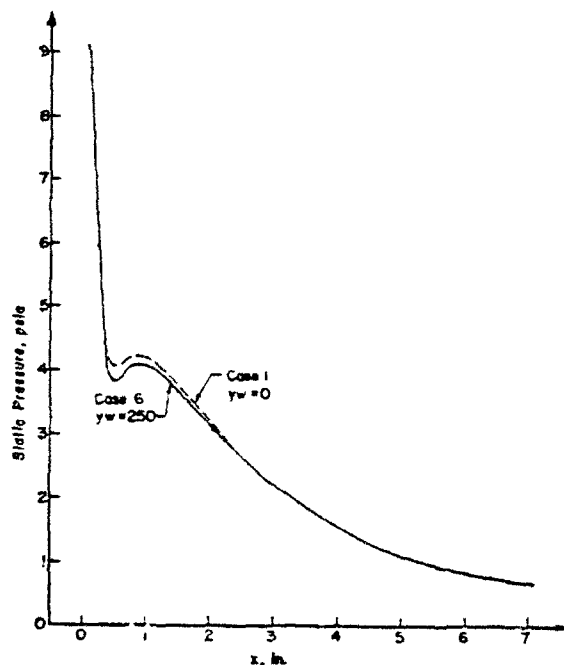

Fig. 11. Pressure distributions on the cowl for Cases 1 and 6.

Table 2 summarizes the mass flow rates, thrusts, and specific impulses for the 12 cases studied. Cases 1 to 6 are for T_o = 2500 R, and Cases 7 to 12 are for T_o = 3500 R. The reference (one-dimensional) mass flow rate for Cases 1 to 6 is m_{1-D} = 21.9842 lbm/sec, and for Cases 7 to 12, m_{1-D} = 18.5800 lbm/sec. Mass flow values were determined by integrating across the initial-value line that is generated from the results of the SNAP analysis. The discharge coefficients are plotted in Fig. 12. The values decrease with increasing swirl in a smooth, consistent manner and indicate consistency in the initial-value data obtained from the SNAP analysis. Thrust values were computed from the results of the method of characteristics (MOC) analysis. The individual thrust contributions from the initial-value line, the cowl, the plug, and the base (illustrated in Fig. 2) are tabulated separately. All values are referenced to zero ambient pressure. The base pressures were computed from Eq. (31).

Fig. 10. Pressure distributions on the plug for Cases 1 and 6.

8

Table 2. Comparison of performance parameters.

Run	Swirl yw (ft^2/sec)	T_o R	Mass Flow (lbm/sec)	C_D	I_{sp} (lbf-sec/lbm)
1	0	2500	21.491	0.9776	141.594
2	50	2500	21.456	0.9760	141.625
3	100	2500	21.350	0.9712	141.665
4	150	2500	21.173	0.9631	141.753
5	200	2500	20.929	0.9520	141.894
6	250	2500	20.611	0.9375	142.161
7	0	3500	18.163	0.9776	167.538
8	50	3500	18.142	0.9764	167.569
9	100	3500	18.078	0.9730	167.602
10	150	3500	17.971	0.9672	167.670
11	200	3500	17.823	0.9593	167.774
12	250	3500	17.633	0.9490	167.952

|			Thrust (lbf)		
Run	Ivl	Cowl	Plug	Base	Total
1	2582.08	298.26	155.34	7.32	3043.00
2	2577.11	298.06	155.57	7.96	3038.70
3	2562.23	297.45	156.28	8.59	3024.55
4	2537.58	296.44	157.53	9.79	3001.34
5	2503.38	295.02	159.37	11.93	2969.70
6	2459.43	292.67	162.17	15.82	2930.09
7	2582.08	298.26	155.34	7.32	3043.00
8	2578.53	298.11	155.51	7.90	3040.05
9	2567.89	297.68	156.01	8.34	3029.92
10	2550.23	296.96	156.88	9.14	3013.21
11	2525.67	295.95	158.17	10.45	2990.24
12	2494.37	294.63	159.87	12.63	2961.50
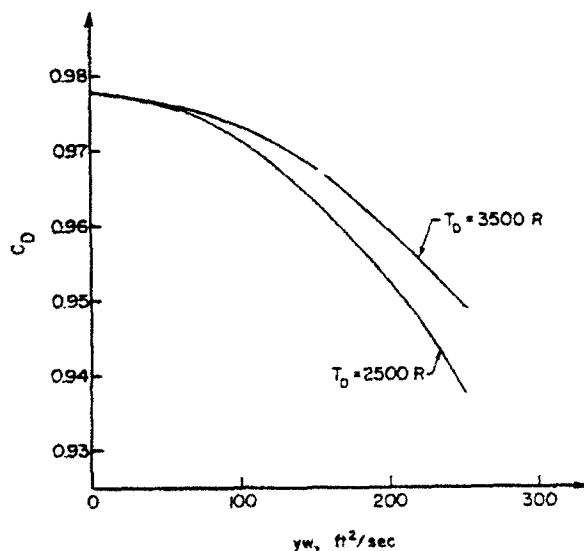
Fig. 12. Discharge coefficients.

The following observations can be made from the results obtained in this study.

1. The data are extremely consistent giving a high degree of confidence in the trends. (We also believe the absolute values are reliable.) The thrust values for Cases 1 and 7 are essentially identical. This is, of course, what one would hope, since changing the stagnation temperature does not affect the absolute thrust values. However, the initial-value line calculated by the CNAP code might be expected to be somewhat different, since the flow speeds and permissible time steps for those calculations are different. This result gives confidence in the consistency of the results.

2. For those applications for which yw < 100 ft^2/sec, the effect of swirl on the mass flow rate and thrust values is very small and can probably be ignored in preliminary design and overall performance considerations. It is probable that this

9

observation is also valid for other than free vortex swirlers.

3. Even at higher swirl values, the specific impulse of the nozzle is not degraded by swirl. The calculations show some increase in I_{sp} with swirl. Therefore, if high swirl is to be used, the effects of swirl on nozzle thrust can be compensated for in the design by increasing the throat area to compensate for the decreased mass flow rate, thus increasing the thrust to the required value without any loss in nozzle efficiency.

4. When the cowl and plug surfaces are contoured to optimize the performance, the optimum contour will probably be affected by the presence of swirl in the flowfield.

Conclusions

An analytical performance prediction methodology for analyzing the effects of swirl in annular propulsive nozzles has been developed. Computed results for a series of swirl intensities for free vortex swirlers are extremely consistent and indicate a high reliability in the results. Swirl decreases the discharge coefficient of a nozzle but has very little effect on the vacuum specific impulse.

For swirl intensities often encountered in ramjet and turbojet applications, the effect of swirl on the nozzle performance is small, and can probably be neglected in preliminary design and performance calculations.

Experimental verification of the results is needed. Application of the methodology to other than free vortex swirlers is needed.

References

1. Buckley, P.L., Craig, R.R., Davis, D.L., and Schwartzkopf, K.G., "The Design and Combustion Performance of Practical Swirlers for Integral Rocket/Ramjets," AIAA Journal, Vol. 21, No. 5, pp. 733-740, May 1983.

2. Scharrer, G.L. and Lilley, D.G., "Five-Hole Pitot Probe Measurements of Swirl, Confinement and Nozzle Effects on Confined Turbulent Flow," AIAA Paper 84-1605, June 1984.

3. Conley, Ralph R., Hoffman, Joe D., and Thompson, H. Doyle, "An Analytical and Experimental Investigation of Annular Propulsive Nozzles," AIAA Paper 84-0282, January 1984.

4. Dutton, J. Craig, "Time-Dependent Calculations of Swirling Nozzle Flow," Final Report, 1983 USAF-SCEEE Summer Faculty Research Program, Air Force Office of Scientific Research, August 11, 1983.

5. Zucrow, M.J. and Hoffman, J.D., Gas Dynamics, Vol. 1, Chapter 10, John Wiley and Sons, New York, 1975.

6. Cline M.C., "VNAP: A Computer Program for Computation of Two-Dimensional, Time-Dependent, Viscous, Internal Flow," Report LA-7326, Los Alamos Scientific Laboratory, Los Alamos, NM 87545, November 1978.

7. MacCormack, R.W., "The Effect of Viscosity in Hypervelocity Impact Cratering," AIAA Paper 69-354, April 1969.

8. Kornblum, B.T. and Thompson, H.D., "A Method of Characteristics Program for Computing Annular Nozzle Flowfields with Swirl," Report ME-TSPC-84-01, Thermal Sciences and Propulsion Center, Purdue University, West Lafayette, IN, July 1984.

AIAA-86-0587

An Analytical Investigation of the
Effects of Swirler Design on the
Performance of Annular
Propulsive Nozzles

J. D. Hoffman, H. D. Thompson
and D. L. Marcum, Purdue Univ.,
West Lafayette, IN

AIAA 24th Aerospace Sciences Meeting
January 6-9, 1986/Reno, Nevada

AN ANALYTICAL INVESTIGATION OF THE EFFECTS OF SWIRLER DESIGN

ON THE PERFORMANCE OF ANNULAR PROPULSIVE NOZZLES

Joe D. Hoffman[+], H. Doyle Thompson[*] and David L. Marcum[#]
Purdue University
West Lafayette, Indiana 47907

Abstract

An analytical performance prediction methodology for annular propulsive nozzles with swirl introduced in the combustor upstream of the nozzle is presented. The methodology is applied to investigate the effects of swirler design on the performance of annular propulsive nozzles. Four types of swirlers were investigated: free vortex, constant angle, forced vortex, and Rankine vortex swirlers. Discharge coefficients, specific impulses, and wall pressure distributions are presented. These numerical studies show that the discharge coefficient, the thrust, and the vacuum specific impulse decrease as the amount of swirl increases, but that the decrease in specific impulse is modest. The effect of swirl on the discharge coefficient, for all four swirler designs, correlates well with the mass-averaged swirl introduced into the flowfield by the swirler. However, the decrease in vacuum specific impulse is a function of the swirler design. The forced vortex swirler has the least decrease in specific impulse with increasing swirl while the free vortex swirler has the greatest decrease. This methodology will enable nozzle designers to account for the effects of swirl in nozzle design.

Nomenclature

a	speed of sound
C_1-C_4	constants specifying tangential velocity distributions
C_5-C_8	constants used to set the mass flow rate
F	thrust
$\dot{m}$	mass flow rate
M	Mach number
P, P_0	static and stagnation pressure, respectively
R	gas constant
S	swirl number
t	time
T, T_0	static and stagnation temperature, respectively
u, v, w	velocity components
V	velocity magnitude
x, y	axial and radial coordinates, respectively
$\overline{yw}$	mass-averaged swirl
Y_1, Y_2	inner and outer radii of the flow passage, respectively
γ	specific heat ratio
ρ	density
θ	tangential coordinate
ζ, η, ψ	transformed coordinates

Subscripts

A to F	geometric stations
B,C,P,IVL	base, cowl, plug, and initial-value line, respectively

Introduction

Recent studies indicate that the introduction of swirl ahead of the combustor in axisymmetric dump combustors can have very beneficial effects on the combustion process. Buckley, Craig, Davis and Schwartzkopf[1] found that swirl both reduced the reattachment length of the combustor flowfield (thereby reducing the overall combustor length needed for good performance), and helped eliminate destructive very low frequency instabilities. They further concluded that (in the range of swirl intensities of their study) "losses in thrust due to residual swirl, at least to the sonic point of the nozzle, are negligible."

Scharrer and Lilley[2] made five-hole pitot probe measurements of the effects of swirl in simulated dump combustors followed by a nozzle. They observed a significant interaction between the swirling flowfield in the simulated combustor and the nozzle flowfield. Their major objective, however, was the measurement of the confined turbulent flow in the simulated combustor, not the nozzle flowfield. Consequently, their nozzles were simply used as downstream blockage components. Both nozzles used in their studies were conventional converging nozzles without centerbodies.

Conley, Hoffman and Thompson[3] presented an analytical and experimental investigation of the performance of annular propulsive nozzles without swirl. Kornblum, Thompson, and Hoffman[4] extended the performance prediction methodology developed by Conley et al. to include the effects of swirl introduced in the combustor on the performance of annular propulsive nozzles for free vortex swirlers. A similar study performed by Dutton[5] shows trends similar to the results obtained by Kornblum, et al. for conventional converging-diverging nozzles without centerbodies.

The present work is an extension of the performance prediction methodology developed by Kornblum, Thompson, and Hoffman[4] to include constant angle swirlers, forced vortex swirlers, and Rankine vortex swirlers.

[+] Professor of Mechanical Engineering. Thermal Sciences and Propulsion Center. Member AIAA.

[*] Professor of Mechanical Engineering. Thermal Sciences and Propulsion Center. Associate Fellow AIAA.

[#] Research Assistant in Mechanical Engineering. Member AIAA.

1

Performance Prediction Methodology

Geometric Model

The geometric model considered in this investigation is presented in Fig. 1. Air enters at Station A and flows through a swirler where tangential momentum is transferred to the air to give the desired tangential velocity distribution at Station B. Station B is followed by a sudden expansion dump into the combustor inlet at Station C. Combustion takes place between Stations C and D, where the stagnation temperature T_0 rises corresponding to the amount of fuel added, and the stagnation pressure P_0 decreases slightly due to friction, mixing, and heat addition. The combustion products accelerate in the nozzle to the choked condition at the nozzle throat, Station E, after which the flow continues to accelerate supersonically from Station E to Station F.

The concern in the present study was the effect of swirl induced in the swirler on the performance of the nozzle (i.e., mass flow rate, thrust, and specific impulse). Consequently, the swirler, the sudden expansion dump, and the combustor are not modeled in detail in the present analysis. Emphasis is placed on the nozzle flowfield. The swirl introduced by the swirler is assumed to flow through the combustor and nozzle unchanged in magnitude.

Performance Model

Figure 2 illustrates the thrust producing components of a generic annular nozzle. The nozzle thrust is composed of the thrust developed across the initial-value line F_{IVL}, the thrust developed by the pressure acting on the cowl F_C, the thrust developed by the pressure acting on the plug F_P, and the thrust acting on the plug base F_B. Thus, the pressure distributions along the cowl and the plug and the base pressure must be calculated to enable the calculation of the nozzle performance.

Swirler Model

The swirler is a set of axial flow guide vanes that imparts the desired tangential velocity distribution to the air as it passes through the swirler, that is, from Section A to Section B in Fig. 1. Buckley, Craig, Davis, and Schwartzkopf[1] experimentally investigated four types of tangential velocity distributions at the swirler exit. They are:

Free vortex: $\quad w = C_1/y$ $\qquad\qquad$ (1)

Constant angle: $\quad w = C_2 u = u \tan \alpha$ $\qquad$ (2)

Forced vortex: $\quad w = C_3 y$ $\qquad\qquad$ (3)

Rankine vortex: $\quad w = (C_4/y)[1 - \exp(-y^2/Y_2^2)]$ $\quad$ (4)

where the constants C_1 to C_4 are specified to achieve the desired tangential velocity distribution. In the present study, all four swirler types were considered.

For an axially symmetric combustor and nozzle without friction or obstructions, the tangential momentum equation reduces to

$$D(yw)/Dt = 0 \qquad (5)$$

which is the substantial derivative form of the equation. For steady flow, Eq. (5) requires that the swirl yw remain constant on a streamline. Thus, the swirl, yw, as a function of the stream function, is the same throughout the flowfield from Station B (the swirler exit) to Station F (the nozzle exit). Furthermore, the mass-averaged swirl, $\overline{yw}$, is the same at all stations from the swirler exit to the nozzle exit, where

$$\overline{yw} = \frac{1}{m} \int_{Y_1}^{Y_2} yw \; dm = \frac{1}{m} \int_{Y_1}^{Y_2} yw \; \rho u \, 2\pi y \, dy \qquad (6)$$

The swirl distribution at the nozzle inlet, Station D, is determined as follows. The swirl distribution at the swirler exit, Station B, is calculated as a function of the fractional mass flow rate. That same swirl distribution is specified at the nozzle entrance, Station D, as initial conditions for the transonic flow analysis. The swirl distribution at Station B is computed as a function of the fractional mass flow rate as follows:

(a) The stagnation temperature and pressure at the swirler inlet, Station A, are assigned.

(b) The radial velocity component v is assumed to be zero, so that the radial momentum equation reduces to

$$dP/dy = \rho w^2/y \qquad (7)$$

(c) The pressure-velocity relationship specified by Bernoulli's equation is assumed to be valid.

$$dP = -\rho V \, dV \qquad (8)$$

This is an approximation for the constant angle, the forced vortex, and the Rankine vortex swirlers.

(d) Equations (7) and (8) are combined with the appropriate swirler relationship, Eq. (1), (2), (3) or (4), to relate the velocity components to a constant. The constant is set by matching the desired mass flow rate as described in step (e) below. For the free vortex swirler, the axial velocity component u must be constant.

$$u = C_5 \qquad \text{(free vortex)} \qquad (9)$$

For the constant angle swirler,

$$V y^k = C_6 \qquad \text{(constant angle)} \qquad (10)$$

where $k = \sin^2\alpha$, and α is the swirl angle in Eq. (2). For the forced vortex swirler,

$$u^2 + 2w^2 = C_7 \qquad \text{(forced vortex)} \qquad (11)$$

where w is related to y by Eq. (3). For the Rankine vortex swirler, the following integral relationship is obtained.

$$\int_{C_8}^{V} V \, dV = \int_{Y_1}^{y} (w^2/y) dy \qquad (12)$$

where C_8 is the velocity magnitude at the inner radius and w is a function of y as specified by Eq. (4). The value of C_8 is determined iteratively to give the specified mass flow rate at Station B.

(e) The mass flow rate is calculated using the discharge coefficient versus swirl results for free vortex swirlers in Ref. (4).

(f) The mass-averaged swirl $\overline{yw}$ is set by the values of the constants in Eqs. (1) to (4). Thus, the value of C_1 in Eq. (1) sets the swirl for a free vortex swirler; the value of C_2 in Eq. (2) determines the swirl for a constant angle swirler; the value of C_3 in Eq. (3) determines the swirl for a forced vortex swirler; and the value of C_4 in Eq. (4) determines the swirl for a Rankine vortex swirler.

(g) The mass flow rate at Station B is determined by numerically integrating

$$m = 2\pi \int_{Y_1}^{Y_2} \rho u y \, dy \qquad (13)$$

The mass flow rate is a function of the constant C_5 in Eq. (9) for the free vortex swirler, of the constant C_6 in Eq. (10) for the constant angle swirler, of the constant C_7 in Eq. (11) for the forced vortex swirler, and of the integration limit C_8 in Eq. (12) for the Rankine vortex swirler. Iteration for the constants is required to match the mass flow rate in Step (e).

(h) Equation (6) is numerically integrated to determine the swirl intensity $\overline{yw}$. Convenient values of $\overline{yw}$ are obtained by iterating on the constants C_1 to C_4 in Eqs. (1) to (4).

(i) A table of yw versus fractional mass flow rate at Station B is calculated. As required by Eq. (5), that relationship between yw and fractional mass flow rate also applies at all other sections in the flow, and specifically at Station D. That relationship provides the needed initial conditions for the transonic flow computations described below.

(j) The transonic flow calculations provide an independent determination of the choked mass flow rate through the nozzle. If the mass flow rate determined from the transonic flow calculations does not match the value assumed in Step (e), then Steps (e) to (i) can be iterated to convergence.

To provide a basis for comparison of different swirlers, the swirl number S is employed, which is defined as

$$S = \frac{\int_1^{Y_2} \rho u w y^2 \, dy}{Y_2 \int_1^{Y_2} \rho u^2 y \, dy} \qquad (14)$$

Equation (14) is the compressible flow version of the swirl number, and can be numerically integrated to compute the swirl number at Station B, or at any station in the nozzle. The numerator in Eq. (14) is closely related to the mass averaged swirl $\overline{yw}$ in Eq. (6), and is constant at every station in the flowfield. The disadvantage of using the swirl number in this analysis is that the denominator (normalizing integral) in Eq. (14) varies due to changes in both Y_2 and the axial velocity component u, which changes due to both area change and heat addition. Therefore, the swirl number varies rather widely between stations in the flowfield and care must be taken when using the swirl number to compare flows or to correlate data to insure that the values refer to the same station in the flowfield.

Flowfield Model

The accuracy and efficiency of nozzle performance prediction techniques are highly dependent on the flowfield model chosen to represent the actual flowfield. In the present study, the flowfield model is based on the following assumptions: (1) steady axisymmetric flow, (2) inviscid nonconducting fluid, (3) no body forces, (4) thermally and calorically perfect gas, and (5) separation and base pressures predicted from empirical correlations.

The governing equations consist of the continuity equation, the component momentum equations, the energy equation, and the thermal and caloric equations of state. A detailed discussion of these equations is presented in Ref. (6).

The choice of a numerical method, or methods, to solve these governing equations is also crucial to the success of the performance prediction procedure. A subsonic/transonic solution is required to define the mass flow rate and throat thrust, while a supersonic solution is required to define the cowl, plug, and base thrusts. Experience[3] has shown that subsonic/transonic flowfields can be accurately determined from the steady state solution to finite difference time marching solutions, whereas the method of characteristics is the most accurate method for determining supersonic flowfields in nozzles. Therefore, the numerical methods selected for the performance prediction procedure in the present study are a finite difference time marching approach to define the subsonic/transonic flowfield, and a method of characteristics approach to define the supersonic flowfield.

Subsonic/Transonic Flowfield

In the performance prediction methodology developed by Conley, Hoffman, and Thompson[3] for annular nozzles without swirl, the VNAP code (Viscous Nozzle Analysis Program) developed by Cline[7] was used to calculate the subsonic/transonic flowfield. In the performance prediction methodology developed by Kornblum, Thompson, and Hoffman[4], the VNAP code was modified to include the effects of swirl. The resulting program was called SNAP (Swirling Nozzle Analysis Program). Both the VNAP code and the SNAP code are restricted to an equally spaced grid in the axial direction. This is a disadvantage for nozzles having small throat radii of curvature, which is generally the case in annular propulsive nozzles.

In the present investigation, the finite difference code developed by Marcum[8] was used to calculate the subsonic/transonic flowfield. That program solves unsteady, three-dimensional, inviscid flowfields in super-elliptical nozzles with centerbodies. An option exists for calculating unsteady axisymmetric inviscid flowfields in nozzles having circular cross-sections.

The gas dynamic model in Marcum's analysis is based on the following assumptions: (1) unsteady three-dimensional flow, (2) inviscid nonconducting fluid with no body forces, and (3) a simple system in thermodynamic equilibrium. In the present analysis, the fluid was assumed to be a thermally and calorically perfect gas.

3

The analysis is based on the unsteady Euler equations. The finite difference algorithm uses MacCormack's explicit finite difference method[9] at interior points and Kentzer's method[10] at all boundary points. Consequently, the method is capable of predicting both unsteady and steady flowfields. Steady state flowfields are obtained by marching in time until the solution converges to a steady state.

The $xy\theta$ physical space is transformed to the $\zeta\eta\psi$ orthogonal equally spaced computational space by the following algebraic coordinate transformation, which works quite well for a wide variety of internal flows:

$$\zeta = \arctan x \qquad (15)$$

$$\eta = \frac{y - Y_1(x,\theta)}{Y_2(x,\theta) - Y_1(x,\theta)} \qquad (16)$$

$$\psi = \theta \qquad (17)$$

where $Y_2(x,\theta)$ is the cowl radius at a given axial location for a given θ ray, and $Y_1(x,\theta)$ is the corresponding plug radius. The axial transformation permits the clustering of grid lines in the throat region of the nozzle. For an axisymmetric nozzle, $Y_2(x,\theta) = Y_2(x)$ and $Y_1(x,\theta) = Y_1(x)$. The physical grid used in the present study is the 81x21 grid illustrated in Fig. 3.

The initial data, at time $t = 0$, for the velocity magnitude, the pressure, and the density are obtained from a steady quasi-one-dimensional isentropic flow analysis. The initial values of the flow angles are obtained by linear interpolation between the centerbody and the wall. The tangential swirl distribution at the nozzle inlet is specified as a function of the fractional mass flow distribution, $yw = yw(\dot{m})$. This distribution is determined from an analysis of the swirler at Station B. This swirl distribution is used to compute the swirl yw at each point across the nozzle inlet in the following manner. After each time step, the mass flow rate is integrated across the nozzle inlet to determine the fractional mass flow rate at each radial station. The resulting fractional mass flow rate is used to interpolate for the swirl yw at the corresponding computational grid point by quadratic interpolation of the swirl function $yw(\dot{m})$ computed at Station B. The swirl velocity w is computed by dividing the interpolated value of the swirl yw by the value of y at the computational grid point.

Steady state convergence is assumed when the maximum percent change in the flow properties, between successive solution surfaces, is less than 0.001.

Points on an initial-value line along which the projections of the Mach number in the xy plane are supersonic are then specified across the throat region. The initial-value points are carefully chosen so that the initial-value line is spacelike at all points. Iteration on the location of initial-value points is sometimes required. Values of the projected Mach number, flow angle, and tangential velocity along that line are determined by interpolation. Quadratic bivariate interpolating polynomials are fit to the nine closest grid points to each initial-value line point. In this manner, a supersonic initial-value line is determined, which can be used to initiate the solution of the supersonic flowfield by the method of characteristics.

Supersonic Flowfield

The supersonic flowfield is calculated by the method of characteristics for steady two-dimensional flow. The derivation of the characteristic and compatibility equations is a straightforward, although somewhat lengthy, procedure. The derivation is presented by Kornblum and Thompson[11]. The results are not presented here. In brief, three characteristics are determined in the xy plane, the streamline and the right- and left-running Mach lines. Three compatibility equations are determined along the streamline and one compatibility equation is determined along each Mach line. These five compatibility equations are used to solve for u, v, w, P, and ρ. The method is general so that any consistent initial swirl distribution can be treated.

A direct marching method of characteristics procedure is employed to solve the characteristic and compatibility equations. The solution procedure constructs the Mach line network illustrated in Fig. 4. The characteristic and compatibility equations are integrated numerically by the second-order accurate modified-Euler predictor-corrector method. The solution is initiated from the supersonic initial-value line, line TT' determined from the transonic flow analysis. The projected Mach number (in the xy-plane) along the space-like initial-value line must be supersonic. Left-running Mach lines are initiated from line TT', starting at point T, and continued across the flowfield until they intersect the cowl contour TE. The last such Mach line from point T' intersects the cowl at point T". Left-running Mach lines are then initiated from points on the centerbody and continued across the flowfield to intersect the nozzle wall. This procedure is continued until the nozzle exit lip point, point E, is determined. Left-running Mach lines are then terminated at the last right-running Mach line emanating from Point E. This procedure is continued until point F, at the end of the plug, is determined. When Mach lines of the same family coalesce, embedded shock waves are formed. In the computer program, when Mach lines coalesce, one of the Mach lines is discontinued. This procedure works well for weak shock waves.

The base pressure on the face of the truncated plug is computed from the empirical correlation proposed by Johnson[12]:

$$P_{base} = 0.846\, P_f / M_f^{1.3} \qquad (18)$$

It should be noted that Eq. (18) only fits measured data when the base area is small. It gives unrealistically high values for highly truncated plugs and for expansion-deflection nozzles.

The above procedure determines all of the data required to evaluate the thrust components illustrated in Fig. 2.

Results

Nozzle flowfields were computed for the 13 cases defined in Table 1. Figure 5 defines the flowfield geometry for all 13 cases. The swirl strength was characterized by selected values of the mass-averaged swirl $\overline{yw}$. Values of $\overline{yw}$ of 0 (the no swirl case), 50, 100 and 150 ft²/sec for the free vortex swirler, of 50, 100, 150 and 175 ft²/sec for the constant angle swirler, of 50, 100, and 125 ft²/sec for the

forced vortex swirler, and of 50 and 100 ft²/sec for the Rankine vortex swirler were analyzed. Stagnation temperature and pressure at the nozzle inlet were 2500 R and 35 psia, respectively. In all cases, the specific heat ratio $\gamma = 1.40$ and the gas constant $R = 53.35$ (ft-lb)/(lbm-R). The values of swirl chosen represent the practical range for the geometry and temperature chosen here. Higher values of swirl result in supersonic Mach numbers at the swirler exit and were therefore not considered.

The compressible swirl number S, defined by Eq. (14), varies with axial location in the flowfield. Table 1 gives approximate values of S at Stations B, D and E as determined by numerical integration of Eq. (14) for each case.

Figure 6 presents constant Mach number contours in the transonic region for Case 1 (no swirl) as computed by the transonic flow analysis. Comparison with the constant Mach number contours for the other 12 cases show insignificant differences. Thus, Fig. 6 is representative of the plots for all 13 cases. There are some minor differences, however, which are discernible in the integrated mass flow rate values and thrust values.

Figure 7 compares the static pressure distributions on the plug for Cases 1, 4, 8, 11, and 13. There is a pressure decrease on the plug due to the effects of swirl. The decrease is greatest for the free vortex swirler and least for the forced vortex swirler. The pressure distributions for the intermediate values of swirl for each swirler design lie between the results presented in Fig. 7 in a very orderly fashion.

Figure 8 presents the pressure distributions on the cowl. The pressure distributions on the cowl are almost indistinguishable for all 13 swirl values. However, there are some minor differences in the values of cowl, plug, and base thrusts.

Table 2 summarizes the mass flow rates, discharge coefficients, and specific impulses for the 13 cases studied. The reference (one-dimensional) mass flow rate is 21.984 lbm/sec. Mass flow rate values were determined by integrating across the initial-value line that is generated from the results of the transonic analysis. The zero swirl discharge coefficient (0.9853) reflects the two-dimensional nature of the flowfield and is a function of the transonic geometry. The discharge coefficients are presented in Fig. 9 as a function of mass-averaged swirl $\overline{yw}$. The values decrease with increasing swirl in a smooth, consistent manner and correlate very well for all four swirler types. The results indicate a high degree of consistency in the initial-value data.

Figure 10 presents the vacuum specific impulse as a function of mass-averaged swirl. The results indicate that the decrease in vacuum specific impulse is a function of swirler design, and is least for forced vortex swirlers and greatest for free vortex swirlers. In fact, the decrease for the forced vortex swirlers is very small. This result suggests a preference for forced vortex swirlers as far as nozzle performance is concerned, all other factors being equal. The specific impulses of the constant angle and Rankine vortex swirlers lie between the values for the forced and free vortex swirlers. Notice that the vacuum specific impulse scale is large, so that the decrease in the worst case is only 0.35 percent.

In most cases of interest for ramjet or turbojet applications, the values of the mass-averaged swirl $\overline{yw}$ are no more than about 100 ft²/sec, and the effect of swirl on the nozzle performance is small and can probably be neglected in preliminary design and overall performance calculations.

The individual thrust contributions from the initial-value line, the cowl, the plug, and the base (illustrated in Fig. 2) are tabulated separately in Table 3. The thrust values are computed from the method of characteristics (MOC) analysis and all values are referenced to zero ambient pressure.

The following observations regarding the effect of swirl in annular nozzles can be made from the results obtained in this study.

1. The data are extremely consistent, giving a high degree of confidence in the trends.

2. The effects of swirl on discharge coefficient correlate well with the mass-averaged swirl $\overline{yw}$ for the different swirlers.

3. The effects of swirl on the vacuum specific impulse are a function of swirler design. The loss in vacuum specific impulse is least for forced vortex swirlers and greatest for free vortex swirlers.

4. For those applications for which $\overline{yw} < 100$ ft²/sec, the effect of swirl on the mass flow rate, the thrust, and the vacuum specific impulse is small and can probably be ignored in preliminary design and overall performance considerations.

5. At higher values of swirl, the overall thrust is significantly decreased by the effects of swirl. In some cases, part of the thrust decrease can be recovered by increasing the throat area to compensate for the decreased mass flow rate. When geometric constraints restrict the nozzle exit area, such a design change may not produce the overall desired result. In any case, there is a real loss in specific impulse that cannot be recovered.

6. When the cowl and plug surfaces are contoured to optimize the nozzle performance as, for example, in Ref. (12), the optimum contour will be affected by the presence of swirl in the flowfield.

Conclusions

An analytical performance prediction methodology for predicting the effects of swirl in annular propulsive nozzles has been developed. Computed results for a series of swirl values for free vortex, constant angle, forced vortex, and Rankine vortex swirlers are extremely consistent and indicate a high reliability in the results. Swirl decreases the discharge coefficient, the thrust, and the vacuum specific impulse. The decrease in discharge coefficient correlates with the mass averaged swirl $\overline{yw}$ for all four types of swirlers. The decrease in vacuum specific impulse is a function of the swirler design and is least for forced vortex swirlers and greatest for free vortex swirlers. For values of swirl often encountered in ramjet and turbojet applications, the effect of swirl on the nozzle performance is small and can probably be neglected in preliminary design and overall performance calculations. Experimental verification of these conclusions is needed.

References

1. Buckley, P.L., Craig, R.R., Davis, D.L., and
   Schwartzkopf, K.G., "The Design and Combustion
   Performance of Practical Swirlers for Integral
   Rocket/Ramjets," AIAA Journal, Vol. 21, May 1983,
   pp. 733-740.

2. Scharrer, G.L. and Lilley, D.G., "Five-Hole Pitot
   Probe Measurements of Swirl, Confinement and
   Nozzle Effects on Confined Turbulent Flow," AIAA
   Paper 84-1605, June 1984.

3. Conley, R.R., Hoffman, J.D., and Thompson, H.D.,
   "An Analytical and Experimental Investigation of
   Annular Propulsive Nozzles," AIAA Journal of
   Aircraft, Vol 22, April 1985, pp. 270-276.

4. Kornblum, B.T., Thompson, H.D., and Hoffman,
   J.D., "An Analytical Investigation of the Effects of
   Swirl on Annular Propulsive Nozzles," AIAA Paper
   85-0364, January 1985.

5. Dutton, J.C., "Time-Dependent Calculations of
   Swirling Nozzle Flow," 1983 USAF-SCEEE Summer
   Faculty Research Program, Air Force Office of
   Scientific Research, Final Report, August 12, 1983.

6. Zucrow, M.J. and Hoffman, J.D., Gas Dynamics,
   Vol. 1, John Wiley and Sons, New York, 1975,
   Chapter 10.

7. Cline M.C., "VNAP: A Computer Program for
   Computation of Two-Dimensional, Time-Dependent,
   Viscous, Internal Flow," Los Alamos Scientific
   Laboratory, Los Alamos, NM, Report LA-7326,
   November 1978.

8. Marcum, D.L., "Calculation of Unsteady Three-
   Dimensional Inviscid Flowfields in Nozzles with
   Centerbodies," Ph.D. Thesis, Purdue University, West
   Lafayette, IN, August 1985.

9. MacCormack, R.W., "The Effect of Viscosity in
   Hypervelocity Impact Cratering," AIAA Paper 69-
   354, April 1969.

10. Kentzer, C.P., "Discretization of Boundary Conditions
    on Moving Discontinuities," Second International
    Conference on Numerical Methods in Fluid
    Dynamics," Berkeley, California, September 1970.
    Published in Lecture Notes in Physics, Vol. 8,
    Springer-Verlag, New York, pp. 108-113.

11. Kornblum, B.T. and Thompson, H.D., "A Method of
    Characteristics Program for Computing Annular
    Nozzle Flowfields with Swirl," Thermal Sciences and
    Propulsion Center, Purdue University, West
    Lafayette, IN, Report ME-TSPC-84-01, July 1984.

12. Johnson, G.R., "Design of Maximum Thrust Plug
    Nozzles with Variable Inlet Geometry," Ph.D. Thesis,
    Purdue University, West Lafayette, IN, January 1972.

Table 1. Scope of the parametric study

Case	$\overline{yw}$ (ft²/sec)	S_B	S_D	S_I
1[a]	0	0.0	0.0	0.0
2[b]	50	.176	.142	.0473
3[b]	100	.343	.284	.0947
4[b]	150	.494	.424	.1420
5[c]	50	.215	.143	.0476
6[c]	100	.414	.282	.0938
7[c]	150	.594	.424	.1415
8[c]	175	.667	.491	.1644
9[d]	50	.215	.143	.0476
10[d]	100	.407	.280	.0932
11[d]	125	.469	.342	.1150
12[e]	50	.215	.143	.0476
13[e]	100	.395	.282	.0938

a no swirl   d forced vortex
b free vortex   e Rankine vortex
c constant angle

Table 2. Comparison of mass flow and specific impulse.

Case	$\overline{yw}$ (ft²/sec)	Mass Flow (lbm/sec)	C_D	I_{SP} (lbf-sec/lbm)
1[a]	0	21.653	.9849	141.581
2[b]	50	21.617	.9833	141.526
3[b]	100	21.510	.9784	141.359
4[b]	150	21.333	.9704	141.080
5[c]	50	21.619	.9834	141.555
6[c]	100	21.522	.9790	141.455
7[c]	150	21.352	.9713	141.267
8[c]	175	21.248	.9665	141.136
9[d]	50	21.620	.9834	141.566
10[e]	100	21.526	.9792	141.527
11[d]	125	21.459	.9761	141.509
12[e]	50	21.619	.9834	141.565
13[e]	100	21.524	.9791	141.465

a no swirl   d forced vortex
b free vortex   e Rankine vortex
c constant angle

Table 3. Comparison of thrust values

Case	Ivl	Cowl	Plug	Base	Total
1[a]	2595.17	304.46	158.29	7.73	3065.65
2[b]	2590.17	304.23	157.38	7.61	3059.37
3[c]	2575.23	303.46	154.67	7.28	3040.64
4[b]	2550.46	302.21	150.25	6.74	3009.66
5[c]	2590.44	304.85	157.32	7.66	3060.27
6[c]	2576.78	305.57	154.60	7.45	3044.40
7[c]	2553.18	306.02	150.09	7.05	3016.34
8[c]	2538.64	306.05	147.38	6.79	2998.86
9[d]	2590.36	305.42	157.19	7.68	3060.65
10[d]	2576.61	308.37	154.00	7.54	3046.52
11[d]	2566.91	310.56	151.74	7.44	3036.65
12[e]	2590.40	305.19	157.24	7.67	3060.50
13[e]	2575.67	307.53	154.16	7.53	3044.89

a no swirl
b free vortex
c constant angle
d forced vortex
e Rankine vortex

Figure 3. Typical subsonic/transonic flowfield grid
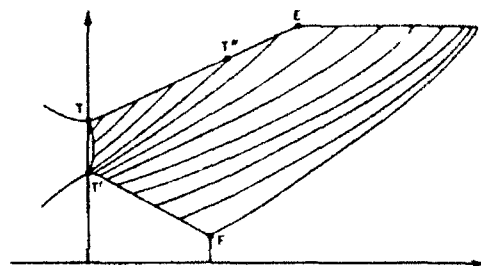
Figure 4. Typical left-running Mach line pattern.

Figure 1. Geometric model.

Figure 2. Thrust producing components of an annular nozzle

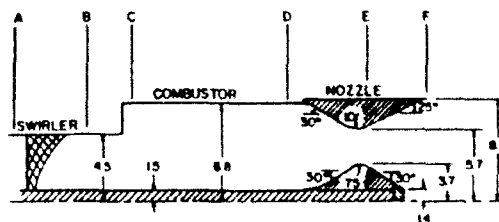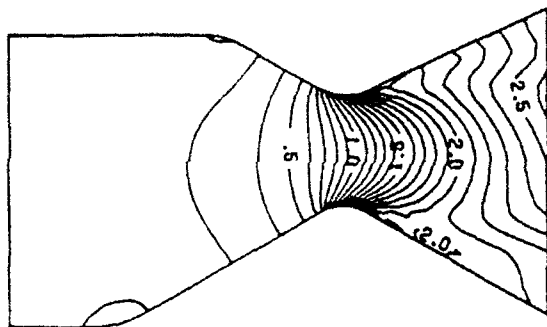Figure 5. Nozzle geometric specifications.

7

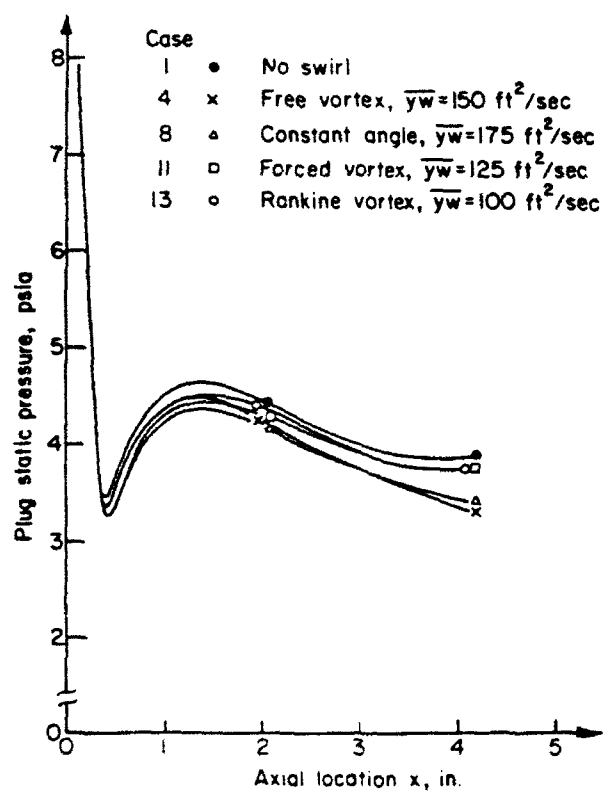Figure 6.   Transonic Mach number distribution for Case 1

Figure 8.   Pressure distributions on the cowl
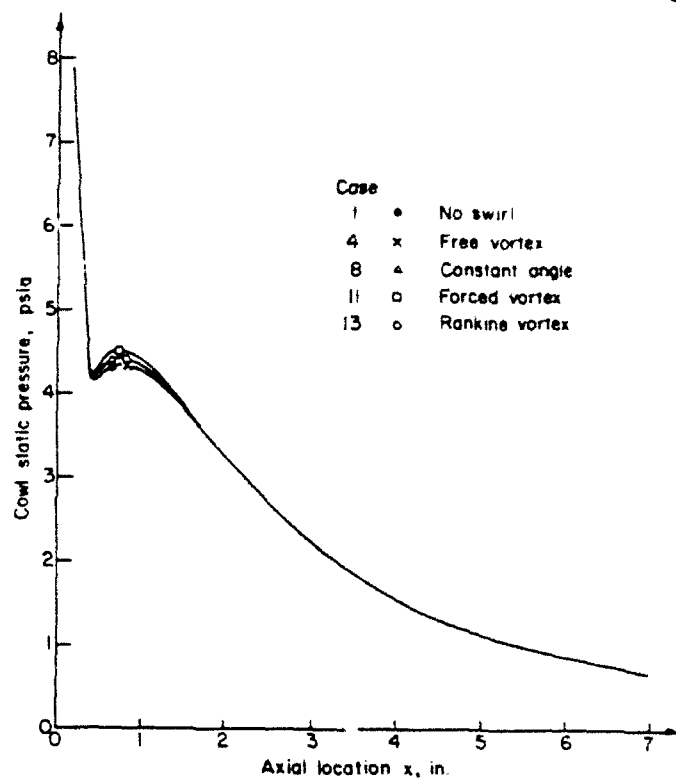

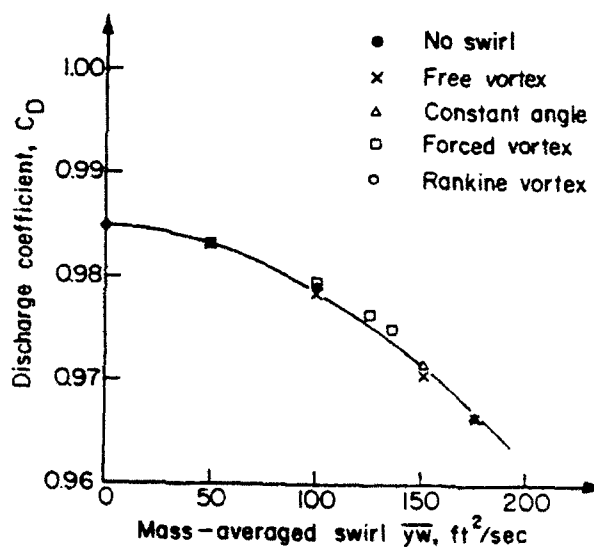Figure 7.   Pressure distributions on the plug.
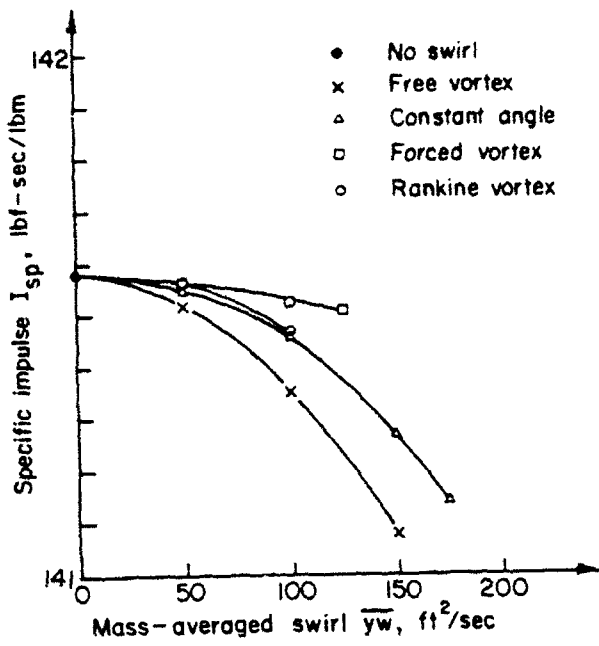

Figure 9.   Discharge coefficients.

Figure 10. Specific impulse comparisons.

-- NOTES --